Journal of
Jnde
Non Destructive Testing
and Evaluation

December 2020
Volume 18 Issue 23

An Official Journal of the Indian Society for Non Destructive Testing

If Undelivered Return To :

Indian Society For Non-Destructive Testing
Module Nos.60 & 61,
Readymade Garment Complex,
Sidco Industrial Estate,
Guindy, Chennai-600032.
Tel: 044-22500412

An ISNT Publication

www.isnt.in

FUJIFILM

Value from Innovation

FUJIFILM DIGITAL RADIOGRAPHY

DYNAMIx™ SYSTEM

MAKING THE INVISIBLE VISIBLE

DYNAMIx™ FXR Pad

DYNAMIx™ FXR

DYNAMIx™ HR²

DYNAMIx™ VU

UR-1

ST-VI

- Superb imaging from the full range of low to high dosage exposures
- High sensitivity, high sharpness and low noise
- Durability for a long expected lifetime

Industrial X-Ray Film IX

- Complaint with Film System Classificat

Fujifilm India Private Limited

Unitech Cyber Park, Unit No. - 801 to 807, 8th Floor, Tower C, Sector 39, Gurugram - 122001, Tel : 0124-4325500

Mumbai Office: 022-42364000 | Bengaluru Office: 080-49332000 | Chennai Office: 044-43994000 | Kolkata Office: 033-40268500

Email: ip@fujifilm.com | Web: www.fujifilm.in

Contents

Journal of Jnde Non Destructive Testing and Evaluation
"Connecting NDT Professionals"
AN ISNT PUBLICATION

DECEMBER 2020
Volume 18 - Issue 23

ON THE COVER Page

Experimental setup for leakage detection.
see article Detection of leakage..Page 17

OBJECTIVE – This Journal of Non Destructive Testing & Evaluation (JNDE) is published quarterly by the Indian Society for Non Destructive Testing (ISNT) for promoting NDT Science & Technology. The objective of this journal is to provide a forum for dissemination of knowledge in NDE & related fields. Papers will be accepted on the basis of their contribution to the growth of NDE Science & Technology.

PUBLISHED BY:- Mr. Rajul R. Parikh - Managing Editor, JNDE

For JNDE SUBSCRIPTION, NEW / RENEWAL OF ISNT MEMBERSHIP INQUIRIES CONTACT:-
Indian Society for Non-Destructive Testing (ISNT)
Modules 60 & 61, 3rd Floor, Readymade Garment Complex, SIDCO Industrial Estate,
Guindy, Chennai – 600 032. India
Tel: 044-2250 0412 / 4203 8175 ***Email: isntheadoffice@gmail.com, info@isnt.in***

For ADVERTISEMENT INQUIRIES CONTACT:-
Rachna Jhaveri - JNDE Executive
8, Jyoti Wire House, 2nd Floor, Off Veera Desai Road, Near Kolsite,
Andheri (W), Mumbai – 400 053. India
Tel : 022 6150 3839 ***Email : isnt.jnde@gmail.com***

LETTERS

PRESIDENT Talk

Dr. B. Venkatraman
President - ISNT
president@isnt.in

As we wish to bid farewell to 2020 to usher in 2021, it is realised that this turn of the calendar is also a right time to reflect on how we fared during 2020 and plan our strategies keeping in view the threats of this pandemic. While 2020 started well with all new visions, the entire world was brought to a near halt by a virus which is just sub micrometers in size. Economies, activities and health have taken a hit which would definitely take time to recover back. While 2020 will go down in our memories as the year of Covid-19 pandemic, this has led to the emergence of digital technologies.

Looking back, 2020 started with our first NGC/NCB meeting of the year as physical meeting at Mahabalipuram and all the subsequent meetings were conducted through video conferencing. Head Office and Chapters of ISNT conducted Series of Webinars, Technical talks, EC meetings, meetings of various committees through Video Conferencing which was a totally new experience to all of us. A major milestone achieved during this year was the accreditation of NCB-ISNT ICN Scheme by NABCB as per the requirement of ISO 17024. For the first time Level III Training courses were conducted online by Mumbai Chapter and the examinations (as per IS 13805) conducted by NCB at different centres to make it convenient for candidates to take the exams without having to travel and undergo hardships. For both these, NCB deserves appreciation.

The Central Conference Committee has toiled and successfully conducted the prestigious and annual flagship event of our Society - NDE 2020 conference cum exhibition as a Virtual Conference providing an online connection to the NDE community around the globe which removed the barriers to traditional attendance--including travel costs, health concerns, etc. This Conference was a grand success with over 600 + delegates, 150+ presentations, 30+ exhibitors and over 40 invited speakers from India and abroad. The same was well appreciated by all the participants, sponsors, exhibitors and other International fraternity.My sincere thanks and gratitude to all members of CCC and also to NGC, Chapter EC and you for this success.I also take this opportunity to thank all Past Presidents and past senior members of NGC and NCB who have always been a source of guidance and support.

It's a time we should cautiously celebrate, the end of year 2020. But many of the problems we experienced in 2020 may continue unless we take the requisite precautions and not repeat the mistakes made. While there is always a talk of second wave, the silver lining in the cloud is the vaccine development. Our goals for this year are clear – implementation of ICN certification, greater scientific and technical activity, improved interfaces with members, industry and corporates and greater visibility at national and international levels. I would like to remind you here that 2020 also happens to be the 125th year of the discovery of X-rays by Roentgen – a brilliant discovery with impact in practically all walks of life and society. We would also celebrate this appropriately in 2021 coupling it with the 125th year of discovery of radioactivity by Henri Becquerel.

Let us join hands, walk together, work as a team and reach our goals for the coming year 2021.

Wishing you, your family and your colleagues a safe, healthy and blissful 2021.

Dr. B. Venkatraman
President

India's Largest Manufacturing Facility
CSIR Approved R&D
NABL Approved Calibration Lab

eeci
the best in ndt

Ultrasonic

- Portable Ultrasonic Flaw Detector
- Phased Array
- Thickness Gauges
- Reference Blocks
- Probes & Accessories
- Rail & Axle Tester



Magnetic Particle

- Prod Units
- Yokes
- Bench Units
- Ultraviolet Black Light
- Consumables & Essentials



Radiography

- Gamma Ray Projectors
- IR-192,Se-75, Co-60 Sources
- Linear Accelerator
- Digital Radiography
- Radiation Detection & Monitoring Devices






Ultrasonic Systems

- On Line / Off Line Systems
- Bar Testing
- Pipe Testing
- Piston Testing
- Component Testing


Eddy Current

- Sorting Equipments
- Component Testing Equipments
- Material Testing Equipments
- Portable Instruments

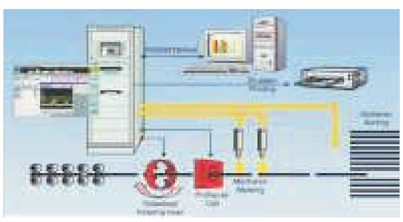


eeci
the best in ndt

ELECTRONIC & ENGINEERING CO. (I). P. LTD

8, 2nd Floor, Jyoti Wire House, Near Kolsite, Off Veera Desai Road, Andheri (W),Mumbai 400 053. India
Tel No.: +91-22-6150 3800 / 26 / 40 ? Fax:- +91-22-6691 9792
Email: ndtsales@eecindia.com ? Web: www.eecindia.com
Regional Offices: CHENNAI, BANGALORE, KOLKATA, HYDERABAD, PUNE, PATNA, NAGPUR, NEW DELHI, VADODARA

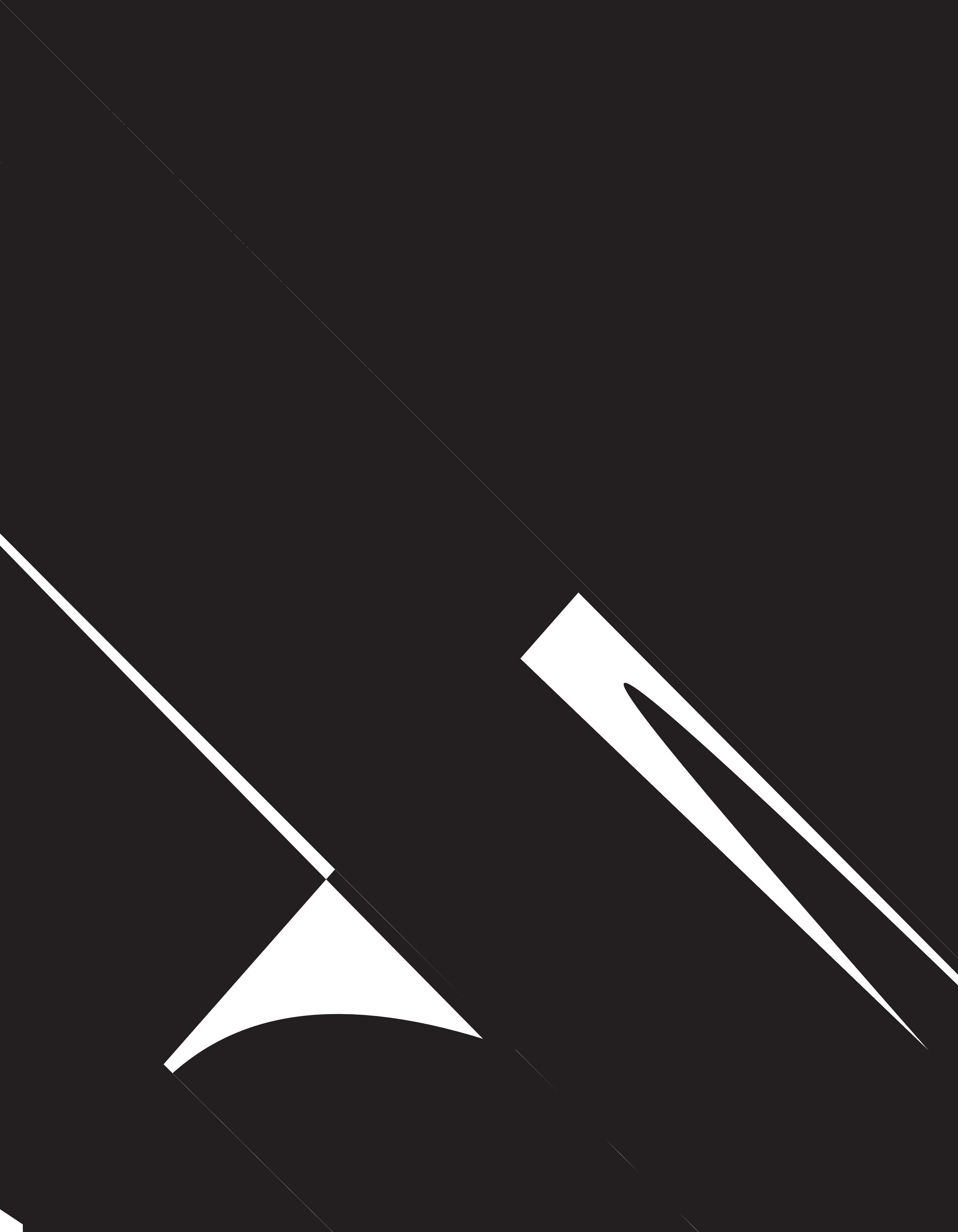

CHAPTER Chairmen & Secretary

AHMEDABAD CHAPTER
Shri Deepak Parikh
Chairman– ISNT-Ahmedabad Chapter
Chairman & Managing Director
Modsonic Instruments Mfg. Co. (P) Ltd.
Plot no. 33, Phase III, GIDC Insustrial Area,
Naroda, Ahmedabad - 382330
Mbl: 9824027282 /
deepak@modsonic.com

Shri Hemant Kumar
Hon. Secretary - ISNT-Ahmedabad Chapter
Head – Reliability Static, CAB-1st Floor, SEZ Refinery,
Reliance Industries Limited,
Jamnagar, Gujarat, India, PIN-361142
(Off)+91 288 6621826 /Cell : 9998215033
hemant.ril2013@gmail.com
/hemantk.kumar@ril.com

BANGALORE CHAPTER
Shri Shri Vedprakash. G
Chairman– ISNT-Bangalore Chapter
Head, Quality Assurance
NUCLEAR POWER CORPORATION OF INDIA LTD
1/1, OLD MADRAS ROAD,
BYAPPANAHALLI,
BANGALORE-560038
PH-9448774943
vedprakashg@rediffmail.com

Shri Shashidhar P. Pallaki
Hon. Secretary, ISNT-Bangalore Chapter
CEO, Pallakki NDT Excellence Center
No-411, A, 4th Phase, Peenya Industrial Area
Bangalore – 560058 / Cell: 0'9448060717
pallakki@pallakkindt.com

CHENNAI CHAPTER
Shri S. Subramanian
Chairman, ISNT - Chennai Chapter,
A-2, ATHREYA SRINIVAS
No.2 (Old No.10), 8th Street,
Nanganallur, Chennai – 600 061
Mb:9444008685
nricsubramanian@gmail.com

Shri. V. Thangamani
Hon.Secretary, ISNT-Chennai Chapter
Senior Manager CPCL
CPCL, Manali, Chennai – 600 060.
Mobile: 9444496808/9445666808
thangam7691@gmail.com /
thangam1969isnt@gmail.com

COIMBATORE CHAPTER
Shri P. Murali
Chairman, ISNT- Coimbatore Chapter
murlinaveen@gmail.com

Shri A. Rathinam
Hon. Secretary, ISNT-Coimbatore Chapter
Cell:0'9843011031
everestndt@gmail.com
isntcoimbatorechapter@gmail.com

DELHI CHAPTER
Shri Raj Kumar Singh
Chairman, ISNT-Delhi Chapter
Cell : 0'9312433853
rajinspection001@gmail.com

Shri F. Siddiqui
Hon. Secretary, ISNT-Delhi Chapter
541/2, Group-I, Hastal, Uttam Nagar,
New Delhi – 110059
Cell: 0'9811466220
isntdelhi@gmail.com /
delhindt@yahoo.com

HYDERABAD CHAPTER
Dr. Jaiteerth R. Joshi
Chairman, ISNT Hyderabad Chapter
Scientist, Project LRSAM, DRDL, Ministry of Defence
Hyderabad-500058, A.P
(Off): 040-24584081 / (Cell): 09440049272
joshidrdl@gmail.com

Shri Surya Prakash Gajjalla
Secretary, ISNT Hyderabad Chapter
CEO, Associated Engineering Services,
Block No. 3-5-944/220-221, 2nd Floor,
Panchavati Mall, Narayanaguda, Hyderabad
Telangana - 500029
Mobile: 09885162668
gajjalla@gmail.com

JAMSHEDPUR CHAPTER
Dr. Sarmishtha P Sagar
Chairman, ISNT-Jamshedpur Chapter
"Senior Principal Scientist & Group Leader
NDE & MM Group," Advanced Materials & Processes Division
CSIR-National Metallurgical Laboratory,
Jamshedpur 831 007
Phone: 0657 2345023 (O),
9431521144 (M)
sarmishtha.sagar@gmail.com /
sarmi@nmlindia.org

Dr. A K Panda
Hon. Secretary, ISNT- Jamshedpur Chapter
akpanda@nmlindia.org

KALPAKKAM CHAPTER
Shri S. Athmalingam
Chairman , ISNT Kalpakkam Chapter,
Associate Director, HSEG & Head - QAD
IGCAR, Kalpakkam - 603 102
Ph: 044-27480071/27480500 (Ext.23490)
Cell:0'9444501819
athma@igcar.gov.in

Shri M.V. Kuppusamy
Hon. Secretary, ISNT Kalpakkam Chapter
Head-QA Projects Section,
Quality Assurance Division, SQ & RMG,
IGCAR, Kalpakkam 603 102
(Off) Phone:044-27480500 Extn. : 22190
Cell:0'8056090071
masikuppu@igcar.gov.in

KOCHI CHAPTER
Shri Sathyan V
Chairman, ISNT- Kochi Chapter
SM (Project), Bharat Petroleum Corp. Ltd.
(Kochi Refinery)
PO Ambalamugal 682 302, Ernakulam, Kochi
0484-2822109 (O)
Cell:0'9446086345
sathyanv@bharatpetroleum.in

Shri Sibi Ignatius
Hon. Secretary, ISNT-Kochi Chapter
BPCL Kochi Refinery,
Ambalamugal - 682302, Ernakulam, Kochi
Ph. No. 0484-2821121 /
Cell:0'9446385611
sibiignatius@bharatpetroleum.in

KOLKATA CHAPTER
Shri Dipankar Gautam
Chairman, ISNT- Kolkata Chapter
AB 121, Salt Lake, Kolkata – 700 064
Ph. No. 033 23581072
Cell: 98048 13030 / 98302 03223
dgautam1956@gmail.com /
dipankargautam@yahoo.co.in

Shri Ambresh Bahl
Chairman, ISNT- Kota Chapter
CE(QA), RR Site, NPCIL, PO - Anushakti,
Via - Kota (Raj) - 323 307
Ph.01475 – 242164 / Cell: 0'9413351764
abahl@npcil.co.in

CHAPTER SPACE

KOTA CHAPTER

Shri A. Varshney
Hon. Secretary, ISNT- Kota Chapter
Sr. Engg. (Quality Assurance),
RAPS – 5&6,
NPCIL, Anu Shakti, Rawatbhata,
Chittorgarh, Rajasthan
Pin-323303 / Cell:9413358365
abhishekvarshney@npcil.co.in

MUMBAI CHAPTER

Shri P. P. Nanekar
Chairman – ISNT Mumbai Chapter
Quality Assurance Division,
BARC, Trombay, Mumbai – 400 085
Off: 022-25594867 / 25564258
Cell: 0'9892161750
pnanekar@barc.gov.in /
paritoshn@yahoo.com

Shri Samir K. Choksi
Hon. Secretary, ISNT - Mumbai Chapter
Choksi Imaging Ltd., 4 & 5,
Western India House,
Sir P. M. Road, Fort, Mumbai- 400 001
Ph. No. 022-2610 1113 /
Cell: 0'9821011113
Choksiindia@yahoo.co.in

NAGPUR CHAPTER

Shri Jeevan Ghime
Chairman, ISNT-Nagpur Chapter
M/s. Becquerel Industries Pvt. Ltd.
33, Rushikesh Modern Co-op.
Hsg. Society
Ingole Nagar, Wardha Road,
Nagpur - 440005
Cell: 0'9822565879 /
jeevan@biplndt.com

Shri Parag W. Pathak
Hon. Secretary, ISNT - Nagpur Chapter
M/s. NDT Solutions Saket - Pruthvi Appt
Plot No-. A+ B, Second Floor,
Surendra Nagar, Nagpur - 440015
Cell: 0' 7709047371/
paragwpathak@yahoo.com

PUNE CHAPTER

Shri Sunil V Gophan
Chairman –ISNT Pune Chapter
M/s Radiant Quality Services
91/2, Dwarka Kunj, Shop No. 4,
Krishna Colony, Lane No. 10,
Paramhans Nagar, Kothrud,
Pune - 411038
sunilgophan@yahoo.com /
chairman@isntpune.org.in

SRIHARIKOTA CHAPTER

Shri B. Munirathinam
Chairman, ISNT Sriharikota Chapter
General Manager, QCCF, SPROB&SPP
Sriharikota – 524124
(Off) Phone:08623-225711
(Mobile):0'9490439735
bmuni@shar.gov.in
Shri V. Rajasekhar
Hon. Secretary, ISNT Sriharikota Chapter
Chapter Sci/Eng.-SD,NDT,SPP,
SDSC – SHAR, Sriharikota – 524124
Off) Phone:08623-225923
Cell:0'9989898932
rajasekhar.v@shar.gov.in

TARAPUR CHAPTER

Shri N.S. Gulavani
Chairman – ISNT Tarapur Chapter
Outstanding Scientist and Chief
Superintendent,
Tarapur Atomic Power Station-1&2,
Nuclear Power Corporation of
India Limited
Type A-2/21, Anushri Township,
PO: TAPP,
TAL & DIST.: PALGHAR, PIN -401 504
Cell: 0'9422066789 /0'9545436000
nsgulavani@npcil.co.in

Shri Chetan Mali
Hon. Secretary –ISNT Tarapur Chapter
Quality Assurance Section
Tarapur Atomic Power Station 1&2,
NPCIL, PIN -401 504
Cell: 0'9420304188/8806515204
csmali@npcil.co.in /
mali.chetan@rediffmail.com

TRICHY CHAPTER

Shri Revisankaran. U
Chairman, ISNT -Trichy Chapter,
General Manager/Quality BHEL,
Trichy, Tamilnadu, PIN-620014
Cell: 0'9442631219
revi@bhel.in

Dilip Kumar Singh
Hon. Secretary, ISNT -Trichy Chapter,
Deputy Manager, Quality NDTL/ATP
Trichy, Tamilnadu, PIN-620014
Ph. No: 0431 2575826 /
Mb:7845462025
dksingh@bhel.in

TRIVANDRUM CHAPTER

Shri Arumugam M
Chairman-ISNT- Trivandrum Chapter
Group Director, QCNG/SR -LPSC
Valiamala P.O,
Thiruvananthapuram-695547
Ph:0471-256-8053
Cell: 09496020097
m_arumugam@lpsc.gov.in /
arumugamm@rocketmail.com

Shri Shunmugavel A
Hon. Secretary, ISNT- Trivandrum
Chapter
SCI/ENGR SF
QCM/QCG/MME, RFF AREA
VSSC, ISRO P.O.
Thiruvananthapuram - 695022
Ph. No. 0471-2562690 /
Cell: 9249562486
a_shanmugavel@vssc.gov.in /
isnttvm@gmail.com

VADODARA CHAPTER

Shri R. Venkatasubramanian
Chairman-ISNT-Vadodara Chapter
"C/o Industrial X-Ray and Allied
Radiographers India Pvt. Ltd.,"
C-17 / 78, Krishana Industrial Estate,
Opposite to BIDC, Gorwa,
Vadodara – 390 016 Gujarat, India
(O) 0265 – 2280756 / Mb: 9825244941
rmani1511@gmail.com /
chairmanisntvc@gmail.com

Shri Kashyap Niranjan Bhatt
Hon. Secretary, ISNT - Vadodara Chapter
Rushikesh Engineering Resources
306, Vrajsiddhi Tower,
Market Char Rasta,
Rajmahel Road, Vadodara: 390001
GUJARAT, INDIA.
(Mb:) 9825245886
info@rushikeshengg.com /
secretaryisntvc@gmail.com

CHAPTER SPACE

CHAPTER News FOR THE PERIOD FROM OCTOBER 2020 TO DECEMBER 2020

CHENNAI CHAPTER

Courses & Exams Conducted:

Visual Testing Level-II online course was held from 19th October 2020 to 23rd October 2020. Number of candidates attended the course was 18. Mr.R.Balakrishnan was the Course Director. Faculties were Mr.R.Balakrishnan, Mr.M.Manimohan, Mr.S.S.Ananthan, Mr.S.Sundararaman, Mr.S.Velumani and Mr.V.Muralidharan.

Technical Talk:

Technical Talk on "Terahertz NDE: Emerging applications and challenges" by Dr. Bala Pesala,Ph.D., Senior Principal Scientist (CSIR), Professor(AcSIR), Council of Scientific and Industrial Research (CSIR)Central Electronics Engineering Research Institute (CEERI) Chennai, India, was held on 13th September 2020 through Video Conferencing – MS Teams.

Technical Talk on "Pulsed Eddy Current Testing : Theory & Applications"by Mr. Jitender Yadav, Senior Technical Sales Specialist, Eddyfi International – FZE, Dubai, UAE was held on 27th September 2020 through Video Conferencing – MS Teams.

Technical Talk on the topic "Automation of NDT – Opportunities And Challenges" by Dr. CHRISTOPHER LANE, NDT System and Integration Sales Manager, Scientific Solutions Business Division, Olympus Singapore Pte Ltd was held on 18th October 2020 through Video Conferencing – MS Teams.

Technical Talk on "Digital Radiography - Principles And Applications" by Dr. Debasish Mishra, General Electric R&D, and Bangalore was held on 1st November 2020 through Video Conferencing – MS Teams.

Other Activities:

EC Meeting was held on 10th October 2020. Members attended 24 through Google meet video conferencing

E-exam software developed for ISNT CC to conduct a online exam by M/s. ARA software in consultation with Dr. O. Prabhakar and the same software will be implemented during forthcoming courses exam under the supervision of ISNT CC members

ISNT CC has purchased 16 nos. Of various NDT training DVD's from M/s. OP-Tech for our training purposes.

KALPAKKAM CHAPTER

Technical Talk:

Conducted webinar on "Visual Inspection – What An Inspector shall look for" on 10th Oct 2020.

Planned to conduct a webinar on Ultrasonic testing during December 2020.

Other Activities:

- Exclusive website for ISNT Kalpakkam Chapter has been created and made operational
- 3 Life time ISNT members has been added upto September 2020
- Planning to add another 5 members by end of December 2020

KOTA CHAPTER

Technical Talk:

One Technical talk -"Use of Advance NDT in online integrity monitoring of pressure vessels".

Other Activities:

- One executive meeting plus on line discussion
- Level II RT Certificate renewal – One number

MUMBAI CHAPTER

Technical Talk:

Webinar 05/2020, Date: 09th Aug, 2020 Time: 11AM to 1 PM
Topic: Resolution in Radiography and Beyond. Speaker: Dr. Paresh Vaidya

Webinar 06/2020, Date : 23rd Aug,2020 Time: 11 AM to 1 PM
Topic: Non – Destructive Evaluation for material Characterization
Speaker: Dr. Anish Kumar, IGCAR, Kalpakkam.

Other Activities:

The EC Meeting was held on 16th Oct 2020 Virtually on Microsoft meet, 31 EC Members attended the EC Meeting

PUNE CHAPTER

Technical Talk:

Technical Lecture was conducted by Mr. Uday Kale on UT of welds as per AWS D1.1

NDT Webinar was conducted by Mr. Sunil Gophan for GDCTECH Forum of Aluminium Casting.

For their 46 members on 27 October 2020.

Other Activities:

- EC Meeting -8th EC meeting was conducted on on 29th August.
- AGM was conducted on 16th Sept

TRIVANDRUM CHAPTER

22.08.20 : Young Engineers forum lecture (Webinar)

Neutron Radiography by Shri. Girish N Namboodiri, Scientist, NDTF/VSSC

22.08.20 : Young Engineers forum lecture (Webinar)

"Leak Test - Principles & Applications" by Shri. Hafiz KR, Scientist, NDTF/VSSC

Other Activities:

11.07.20 EC Meeting

TRICHIRAPPALLI CHAPTER

Courses Conducted

SNT-TC-1A –level II Certification Course were conducted as mentioned below

Ultrasonic Testing Level-II : Theory 25.08.2020 to 07.09.2020

Practical, Discussion & Exam - 02-11-2020 to 09-11-2020. 27 nos. attended

Other Activities:

- EC Meeting conducted on 05 -11-2020
- Chapter Annual General Body meeting planned for - Virtual Mode Planned on 20-12-2020.
- Accounts Audit Report sent to HO via email on 10-08-2020.
- Detailed chapter report & presentation sent to HO via email on 03-09-2020.

VADODARA CHAPTER

Other Activities:

- At ISNT Vadodara Chapter GST have filed regularly on time and details of the same have forwarded regularly to head office in the year 2020.
- CA audited accounts of ISNT Vadodara Chapter for AY 2020-21 have forwarded to Head Office.
- ISNT Vadodara Chapter has received 10% discount in Propriety Tax for FY 2020-21 by availing relief scheme in Propriety Tax announced by Vadodara Mahanager Seva Sadan.
- Members from ISNT Vadodara Chapter have participated in online programs & meetings conducted by NCB and ISNT time to time.
- NDT Level III (MT) examination was conducted at ISNT Vadodara Chapter on 28-November-2020.

Advance NDT Services

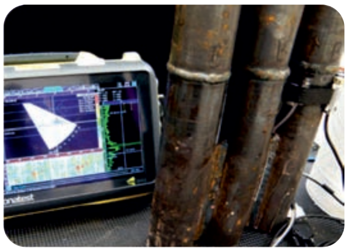

Phased Array Ultrasonic Testing (PAUT)

Thickness Mapping Of
Boiler Tubes With EMAT

High Temperature Thickness Gauging
With EMAT

Remote Visual Inspection/Boroscopy

Tube Testing Solutions
(ECT/RFT/NFT/MFL/ECA)

Corrosion Under Insulation By PECT

ECT Bobbin Probes & Calibration Tubes

Salient Features

- Coils are potted by a wear resistant material
- Stainless steel wear guides at front & rear ends
- Light weight advance polymer kink-resistant cable
- 4-pin Amphenol connector
- Probes available from 12.6 to 47.6 mm
- Cable length available in 15, 20 & 30 metres

Apart from ECT Bobbin probes we also offer calibration tubes in almost materials as per ASME Sec. V Article 8

ARORA
ISO 9001:2015 Certi?ed Company

Arora Technologies (P) Limited
619 & 620 The Great Eastern Galleria, Plot No.20, Sector 4, Nerul, Navi Mumbai 400 706 India
T: +91 22 6138 0600 | E: info@arorandt.com | W: www.arorandt.com

TECHNICAL PAPERS

Estimation of Degree of Moisture Saturation in Cement Concrete Using Electrical Response at Low Radio Frequencies

Gopinandan Dey[1*][0000-0001-5088-0948], AbhijitGanguli[2][0000-0001-8292-4095] and Bishwajit Bhattacharjee[3][0000-0002-6642-9139]
[1]National Institute of Technology Agartala, Agartala, India-799046, Email:gopinita@ymail.com
[2]Indian Institute of Technology Tirupati, Andhra Pradesh, India-517506, Email:abhijit.ganguli@iittp.ac.in
[3]Indian Institute of Technology Delhi, New Delhi, India-110016,Email:bishwa@civil.iitd.ac.in

ABSTRACT

Presence of moisture in the cement based materials (CBM) is the primary cause of deterioration which makes determination of the moisture content an important necessity with regard to health monitoring of concrete structures and characterization of the CBM. The moisture content in CBM is often quantified in terms of the degree of saturation (DoS) which is one of the controlling parameters of the transport phenomenon with implications on durability of the CBM. In this work, a novel electrical technique is proposed for quantification of DoS in cement concrete. Concrete samples of various water to cement ratio (w/c) and dimensions of 75 mm x 75 mm x 300 mm are embedded with electrodes for multiple measurements along the sample length. The AC voltage input are applied at radio frequencies (RF) ranging from 100 kHz to 500 kHz; the variation of the real and imaginary parts of output to input voltage ratio along the length of the sample are investigated with the DoS being homogenized along the sample through treatment in the climate chamber. The electrical responses, measured at various levels of DoS, are found to follow a systematic pattern and a geometric parameter related to the polar plot is presented as an empirical measure of the DoS.

Keywords: Cement concrete, Degree of saturation, Electrical response,Angularparameter, Radio frequency.

Introduction

Cement concrete is the most widely used construction material and can be treated as the backbone of civil infrastructure. It is inherently a porous material and moisture movement through the pores is a common phenomenon owing to its exposure to environment.Due to the presence of moisture in the concrete various deterioration mechanismsof cement based materials (CBM)occur which includealkali-aggregate reaction [1], sulphate attack, corrosion of reinforcement [2], carbonation and chloride attack etc.Therefore, monitoring of the moisture content is important to identify a probable hazardous condition and make contingencies for timely action for prevention of damage.

Considering the importance of estimation of moisture content in CBM many methods have been evolved over last few decades. The prominent among these are nuclear magnetic resonance (NMR) based spectroscopy; attenuation measurement of electromagnetic radiation (e.g. gamma-ray neutron method and X-ray) and electrical methods [3-5]. Electrical methods mostly used for moisture quantification in building materials are based on resistivity measurements. Lataste [6] reported the results of resistivity measurementsby various researchersand concluded that the sensitivity of measurement is good in the 40-80% DoS range. Alsoa DC field stimulates the electrochemical process due to the ionic nature of thecementitious material; howeverthis effect can be minimized by applying an alternating field [7].

AC impedance spectroscopy generates information regarding the real and imaginary parts of the impedance of cementitious materials.Experimental investigation on hardened cement paste [8-9] and saturated cement mortar[10] had been conducted and various RC circuits have been proposed to model the behavior. The real and imaginary parts of impedance of cement pastes are found to be sensitive to the moisture content [9]and thehighest sensitivity of capacitive behaviour is observed from 100 kHz to 1 MHz for asample under various moisture conditions.It is also noted that higher frequencies are more attenuative [11] in a cement paste sample.Therefore,agood correlation can be established between the impedance parameters and the degree of saturation at radio frequencies (RF).

In this paper a technique is presented involving low RF excitation which is similar to AC impedance spectroscopy but differs with regard to the measurement parameters. The technique proposed is able to demonstrate the qualitative electrical response of hardened cement concrete at various moisture saturation conditions and also empirically quantify the degree of saturation (DoS).

Experimental Investigation

Specimen Preparation

Cement concrete specimenswith water to cement ratio (w/c) of 0.45 and 0.55 are prepared, henceforth denoted as CC45 and CC55 respectively. The size of the specimenis 75 mm x 75 mm x 300 mm. Four specimens corresponding to each w/c ratio are cast.Specimens are cast with copper plates of 20 mm x 12.5 mm x 0.4 mm size embedded within a depth of 5 to 6 mm from the exposed surface, at a regular interval of 37.5 mm on all four long faces. Thus, there are seven such plates on each face and altogether 28 plates on a particular specimen. In addition to these two large plates of size 65 mm x 65 mm x 0.4 mm are also embedded on two short faces of each specimen.

The specimens are cast vertically to maintain uniformity in all the four long faces. During casting the bottom plates are embedded directly whereas the top plates are pressed to place in position. After 24 hours the demolding is done and thespecimens are immersed in water and left for 90 days for enhanced curing. After completion of curing the adhesive tapes are removed from the surface of copper electrodes and wires are soldered.

Specimen Conditioning

For this study, a total of sixDoSlevels are considered. These are saturated (designated as DS100) and five partiallysaturated states between87.5% and 37.5% at an interval of 12.5%. The specimensare designated as DS87.5, DS75, DS62.5, DS50 and DS37.5 respectively. Initially the specimensare oven dried at 105±5 ℃ until the constant weightsare achieved and the weights of the specimens are recorded after cooling them to room temperature. The specimensare soaked again in water until the constant weights corresponding to 100% saturationare achieved. Accordingly, the water absorption coefficients are calculated from the difference between dry weight and saturated weight.For CC45and CC55 the obtained values are found to be 6.7% and 8.2% respectively.

To achieve a specific degree of saturation (DoS) in the drying cycle, the specimens are kept in a conditioning chamber at a temperature of 60^{0}C, to avoid any microstructural changes due to high temperature. The weights of the specimens are checked frequently and taken out of the chamber when the desired weight is achieved. Then the specimens are wrapped in a zip-lock polythene bag to avoid further changes in the weight and kept in a conditioning chamber at a temperature of 27^{0}C and 65% RH. The minimum period for which the specimens are kept in the conditioning chamber is 10 days which is conservatively higher than the period (9 days for concrete) as mentioned by Janoo et al. [12] to achieve homogenization of the distribution of the moisture.

Instrumentation and Input Signal

The experimental set-up consists of a Waveform Generator with a maximum frequency range of 20 MHz and a four-channel oscilloscope. The input to the specimensis provided via a coaxial cable having a BNC connector at one end and an alligator clip at the other end. Similar cables are used to connect the sample and the oscilloscope for receiving the output signal. The schematic of the experimental set-up is shown in Fig 1. The experimental set-up and input signals are similar to authors' previous research [13]. However, the electrodes are embedded here contrary to surface electrode used previously.

The input signal is imposed on an electrode on the short end of the specimen and the other end is connected to the ground. Output signals are received at the seven electrode locations on each of the long faces of the specimen. Then the waveform generator is connected to the other end of the specimen and readings are taken in the similar manner at all electrodes on the long faces. Thus eight output signals at a particular distance from the source are obtained as four output can be obtained from four faces of the specimen for each orientation of sample. Hence, altogether fifty six output signals for a specimen corresponding to seven cross sections are obtained. Four specimens are used for each composition in this study thus at a particular cross-section, a total of thirty two signal outputs are obtained.

Direct current which may cause electrolysis and consequently the impairment of the original characteristic of concrete is avoided in the experiment. Thus, a pulse-based excitation (D-Lorentz waveform) is chosen which does not have any DC component. In theinput waveformthe peak to peak amplitude of 10 volts is applied. The output signals are acquired for a time window of 10 μs and digitized by averaging 128 times in the oscilloscope with sampling frequency of 250 MHz.The signals are analyzed in the frequency domain in the -3dB bandwidth,i.e., between100 kHz and 500 kHz.

Data Processing

The acquired time domain signals are converted to frequency domain applying Fast Fourier Transform (FFT) in MATLAB.At selected frequencies between100 kHz and 500

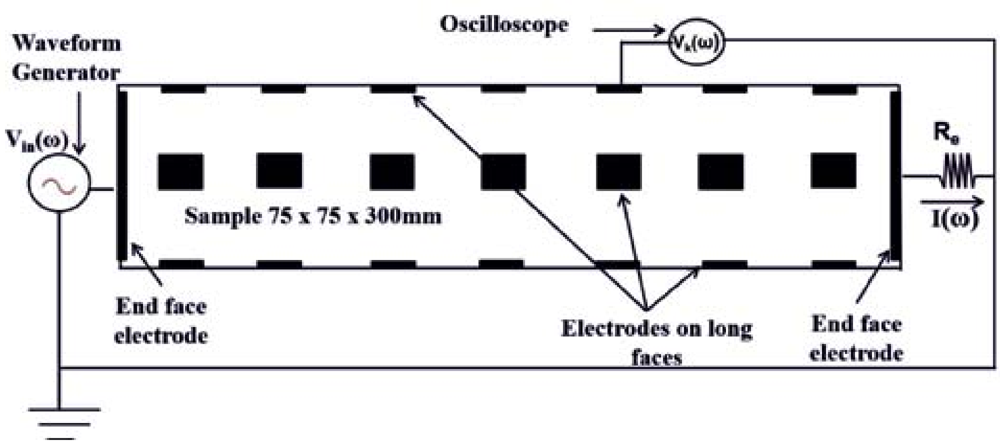

Figure 1 : Experimental set-up[13]

kHz,the ratio between the mean FFT of thirty two output voltages at a particular cross-section and the FFT of the input voltage is obtained. The complex ratio is separated into the real and imaginary parts, henceforth denoted as $V_r^r(\omega)$ $V_r^r(\omega)$ and $V_r^i(\omega)V_r^i(\omega)$ respectively. These parameters are used for estimation of the DoS in this paper. It is presumed that the variation in the output voltage at the four electrodes on the sides of each block at a particular distance from the source for all the four samples of same composition is not very high. Therefore, mean of thirty two values of above two parameters corresponding to each cross section is considered for analysis of experimental results.

Results and Discussion

Converting the time domain signal to frequency domain,voltage at each cross section of the sample is obtained at representative frequencies of 100, 300 and 500 kHz. The ratio between the mean of thirty two output voltages at a particular cross-section and the input voltage is obtained for all the three frequencies. The corresponding values of the $V_r^r(\omega)V_r^r(\omega)$ and $V_r^i(\omega)V_r^i(\omega)$ are considered forfurther analyses.

Variation of Complex Voltage Ratio and Statistical Analysis

Though the specimens are prepared from same batch still there are the some sources of variation in the samples. A little amount of variation in DoSis existed due to change of weight during conditioning and the measurement process. Further, non-uniformity in the contact between every electrode and the material surface, different pore orientation and corresponding pore occupancyare some factors which may lead to the variation of results. A statistical analysis is, therefore,conducted on the output results at various frequencies; however, for brevity a representative result is shown in Fig 2.

The general observation from the figure is that the upper and lower bounds of the 95% confidence interval corresponding to the mean real part vary between ±2 and $\pm$ 4% for the range of DoS studied. However, the confidence interval is comparatively wider for the imaginary parts of the ratio, ranging between ±2 to ±6% of the corresponding mean values. These can be considered significantly low for a heterogeneous material like concrete and the mean value can be used.

Variation of Response with Distance for Different Degrees of Saturation

It is observed that the polar plot between $V_r^r(\omega)V_r^r(\omega)$ and $V_r^i(\omega)V_r^i(\omega)$ for different positions along the length of the sample can be fitted with a straight line for each of the DoS. The fitted lines corresponding to different DoS have different values of gradient as shown in Fig 3.

These straight lines show increase in gradient with a decrease in the DoS. The gradient obtained in each case is

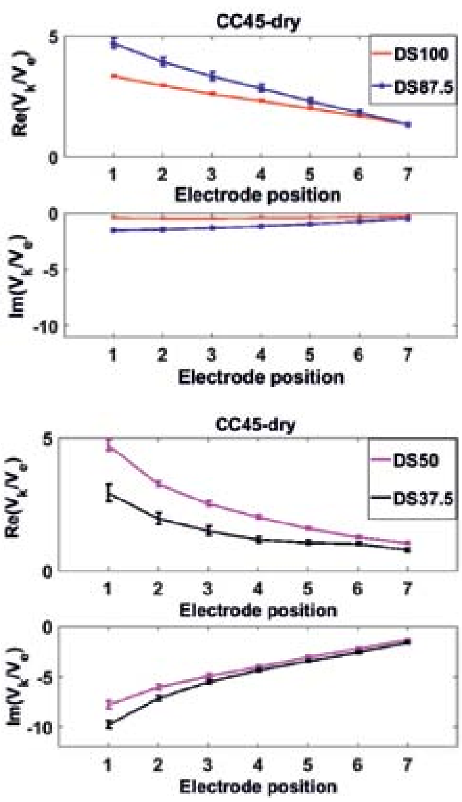

Figure 2 : Error bar showing the spread of 95% confidence interval of real and imaginary parts of the ratio of output voltage and the voltage across the resistance ($V_k/V_e V_k/V_e$) at 300 kHz frequency for CC45 sample

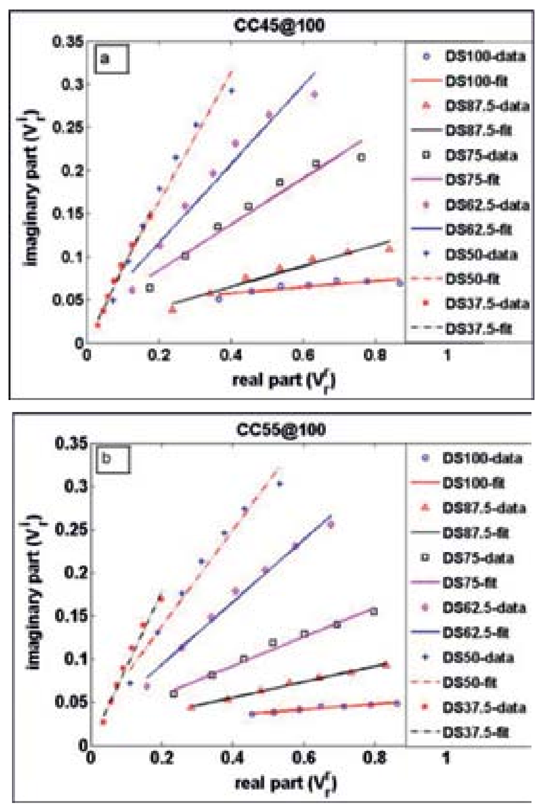

Figure 3 : Polar plot of real vs imaginary parts of voltage ratio $\frac{V_k(\omega)V_k(\omega)}{V_{in}(\omega)V_{in}(\omega)}$ under various DoS and their linear fit along the length for a) CC45 and b) CC55 at excitation frequency 100 kHz

defined as *Angle for Estimation of DoS* and is denoted by 'β'. The behavior of β can be explained as follows. In the present scenario, due to the homogenization, it can be assumed that moisture condition remains approximately same throughout length. Hence, the conductivity and permittivity of the materials are uniform throughout the length and therefore, impedance would vary linearly with the distance. The voltage ratio itself is a function of impedance, as all length segments can be assumed to be in series and current through all length is same for a particular DoS. The real component of the ratio is related to resistance, while imaginary component is inverse of capacitance. Resistance is directly proportional to equivalent resistivity of the system and length of the segment and inversely proportional to equivalent conducting area. The reactance component is also directly proportional to length and equivalent permittivity of the length segment and inversely proportional to equivalent interface area. Therefore, both linearly vary with length, but at different rates for a given DoS. Therefore, plot between real and imaginary parts of voltage ratio exhibits a linear trend for all DoS.

Angular Parameter for Estimation of DoS

In Fig 4 the variation of β as a function of DoS for sample CC45 and CC55 are shown for excitation frequencies 75 kHz to500 kHz. The variation is linear for both the samples at comparatively lower frequencies, wheras at higher frequencies non-linearilty crop up. Though in this study 75 kHz is beyond the -3dB level of input signal it has been considered to show the behavior at lower frequency.

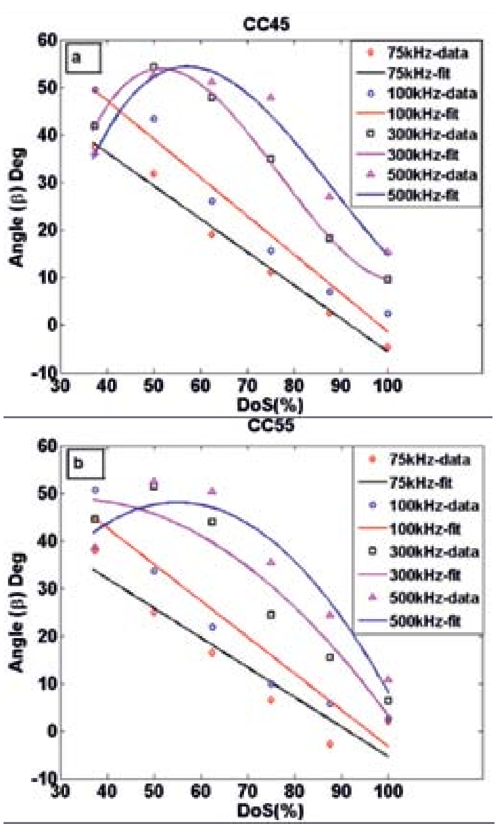

Figure 4 : Variation of angle for estimation of the DoS (β) under various DoS for a) CC45 and b) CC55 at different excitation frequencies

With the increasing frequency, it is seen that the gradient value is reached to a peak at a particular DoS level and then with further decrease of DoS the gradient also decreases, which necessitates fitting with higher order polynomial. This behavior is attributable to the frequency dependency of reactance part of the impedance which has an inverse relationship with frequency. As frequency increases its dominance is reduced, therefore the imaginary part of the ratio decreases. This reduction of imaginary part, without any significant change in real part results in comparatively flatter angle, β thus, there is a reversal of trend. Hence, in order to maintain the simplicity of relationship the results corresponding to 100 kHz is emphasized here and shown in Fig 5.However with proper signal input even lower frequencies can be utilized for establishing a simple linear relationship between angle β and DoS.

In the Fig 4 the graphical representations show the controlled quantity i.e. DoS $(S_w)(S_w)$ in x-axis while the derived quantity i.e. angular parameter $(\beta)(\beta)$ in the y-axis. However, theaim of this research is to estimate the DoS from the electrical parameter. Thus, it would be appropriate to keep the electrical parameter in the x-axis and the dependent variable, DoS in y-axis to enable determination of DoS from angular parameter $(\beta)(\beta)$. Therefore, a revised representation is shown subsequently in Fig 5 at 100 kHz excitation frequency.

The linear variation of the gradient, β with respect to DoS enables to formulate a simple correlation between these two quantities which takes the form of Eq. 1.

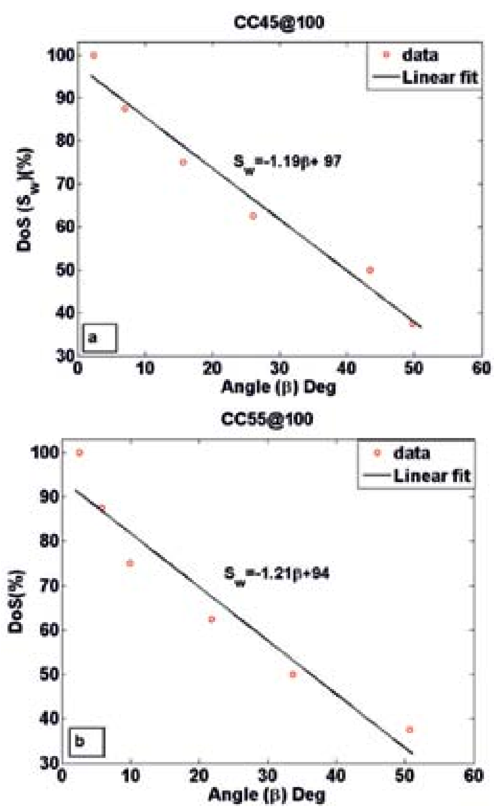

Figure 5 : Relationship between DoS and angle for estimation of the DoS (β) for a) CC45 and b) CC55 at 100 kHz excitation frequency

$S_w = a\beta + b$

where, $S_w S_w$ stands for degree of saturation, aa and bb are the coefficients that depends upon the material composition. In general, it is found that the coefficient aa is around -1.20 for both the mixes and b is close to 100.

Conclusions

In this work a technique has been employed to measure the electrical responseat low RF excitationfor assessment of the grossDoS of a hardened cement concrete specimen. The following conclusions can be drawn with regard to the investigations:

There is a monotonic increase of real part and imaginary part of voltage ratio with distance from the source electrode for all DoS.

The vector plot of real versus imaginary parts of voltage ratio always follows a linear trend having different gradient β at different DoS level.

At lower frequencies the gradient β (named *Angle for estimation of DoS*)increases monotonically with reduction of DoS, however it reduces after reaching to a peak for higher frequencies due to frequency dependency of reactance.

At lower frequency the angle β can be used a measure of DoS with a simplified linear relationship established here.

The study presented here is specific to the materials used. The variation of materials and its effect is not investigated, thus, further investigationswould be carried out to establish generalized results.

References

1. Cyr M, Rivard P, Labrecque F, (2009) Reduction of ASR-expansion using powders ground from various sources of reactive aggregates. CemConcrCompos 31: 438– 446.

2.López W, Gonzalez JA (1993) Influence of the degree of pore saturation on the resistivity of concrete and the corrosion rate of steel reinforcement. CemConcr Res 23: 368-376.

3. Wormald R, Britch AL (1969) Methods of measuring moisture content applicable to building materials. Build Sci3:135-145.

4. Parrott L (1995) A review of methods to determine the moisture conditions in concrete. Performance Criteria for Concrete Durability 294–321.

5.Quincot G, Azenha M, Barros J, Faria R (2011) State of the art–Methods to measure moisture in concrete. Governo da República Portuguesa 1-40.

6.Lataste JF(2016)Electrical investigations for moisture assessment on civil engineering structures. RILEM Proceedings PRO112:203-212.

7. McCarter WJ, Brousseau R (1990) The A.C. response of hardened cement paste. CemConcr Res 20: 891-900.

8.KeddamM, Takenouti H, N´ovoa XR, Andrade C, Alonso C (1997) Impedance measurement of cement paste. CemConcrRes27:1191-1201.

9.Cabeza M, Merino P, Miranda A, N´ovoa XR, Sanchez I (2002) Impedance Spectroscopy study of hardened Portland cement paste. CemConcr Res 32: 881-891.

10.D´ıaz B, Freire BL, Merino P, N´ovoa XR, P´erez MC (2008) Impedance spectroscopy study of saturated mortar samples. ElectrochimActa 53:7549–7555.

11.Dey G, Ganguli A, Bhattacharjee B, Gandhi TK (2016) Electrical behavior of hardened cement paste at radio frequency under various moisture saturation degrees. RILEM Proceedings PRO112:125-134.

12.Janoo V, Korhonen C, Hovan M (1999) Measurement of water content in portland cement concrete. J TranspEng 125: 245-249.

13. Dey G, Ganguli A, Bhattacharjee B (2018) Electrical Conductivity, Dielectric Permittivity, and Degree of Saturation of Cement Mortar at Low Radio Frequencies.Journal of Testing and Evaluation 47:2664-2680.

Detection of Leakage in Pipelines using Passive Acoustic Emission Technique

Nawal Kishor Banjara*, Saptarshi Sasmal and Srinivas Voggu
Special and Multifunctional Structures Laboratory, CSIR-Structural Engineering Research Centre,
Taramani, Chennai-113, India
Email: nawalkishor@serc.res.in/nawal1234@gmail.com

ABSTRACT

Acoustic emission (AE)-based method is a very promising passive measurement technique, because of it's effectiveness in detecting the propagation of acoustic wave signals generated during initiation of micro cracks. Considering the advantage of detecting even the weak emitting acoustic signals for characterizing the fault/damages in the structures, the AE technique is considered to be one of the efficient NDT technique for damage assessment of structures. In the present work, the acoustic emission technique has been utilised to detect leakage in the pipelines by properly analysing the signal parameters for identifying the fault location. High frequency AE sensors are utilised to measure the responses from the pipeline. The leakage in the pipeline is simulated by means of valves provided at identified locations. Sensitivity of the measurements is verified through pencil lead break (PLB) test. Leakage studies in the pipe with a constant water pressure are carried out by slowly releasing the valve at different rate of leakage. AE measurements are captured from the sensors attached to the pipeline and the measured signals are analysed to extract acoustic wave features. The AE features evaluated from the acoustic signals are further processed to identify and localise the leakage (varying flow rate) in the pipe. The features such as AE counts, cumulative AE energy, and signal strength etc. are found to be promising parameters to indicate leakage in the pipe. Results of the study clearly showed that the AE features can effectively be utilized for identifying and localization leakage in the pipeline.

Keywords: Acoustic emission technique, Pipeline, Leakage detection, Flow rates, AE features

1.0 Introduction

For assessment of damage or condition monitoring of any system, it is vital to utilise a non-destructive testing (NDT) technique. The NDT techniques are widely applied to detect internal flaws in the structures and also provide real-time information on the condition of the structure. By definition, non-destructive testing is the technique for evaluation of surface or internal flaws or metallurgical condition in materials or structural components, without interfering with the integrity of the material or it's suitability for service. Various types of NDT techniques such as acoustic emission, thermographic methods, ultrasonic methods, magnetic methods, and vibration analysis for condition assessment are described in [1]. Out of different types of non-destructive techniques, acoustic emission (AE) technique has been found to be one of the most promising and not adequately explored NDT methods for damage/leakage detection, especially for pipelines. The main advantage of this technique is that, it possesses the unique ability to record acoustic events at the moment of initiation of the damage/crack in the structure during service load conditions. This unique quality of the technique allows it's use in structural health monitoring during their service/operational condition. The amount of energy release primarily depends on the size and the speed of the local deformation/flaw or leakage process. Mechanical waves propagate through the solid due to the energy release during the deformations/flaws or leakage process and these waves are detected by the transducers that are located on surface of the specimen as shown in Fig. 1. AE parameters such as energy, count, duration, amplitude, rise time and threshold are the most frequently used AE parameters in the AE testing

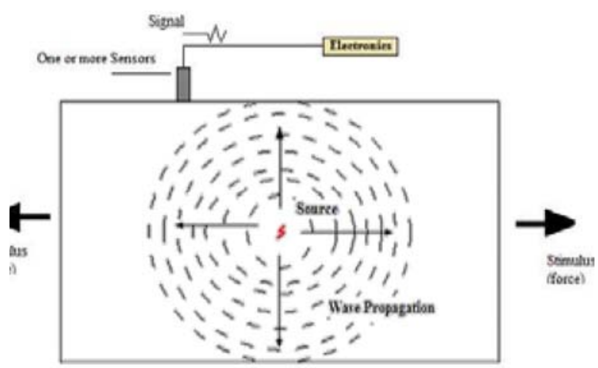

Figure 1 : Concept of acoustic emission technique

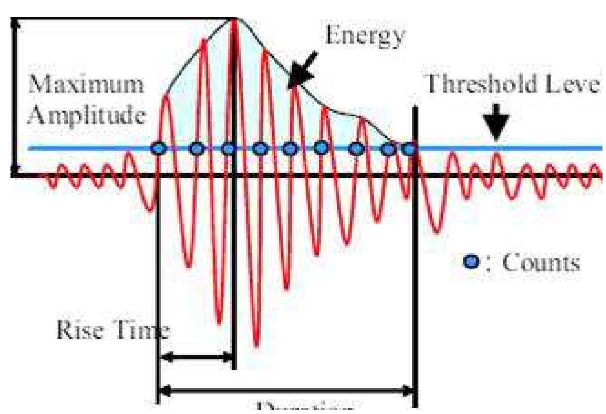

Figure 2 : Parameters involved for acquisition of information from acoustic emission

for identifying or localizing the damage/flaws or leakage in the pipeline system, as shown in Fig. 2.

A leakage in a pipeline system can cause loss in terms of financial, wastage of resources, and even some times human loss due to the failure of the pipelines. Many approaches were introduced to identify and diagnose leakage in the pipeline. Acoustic emission (AE)-based techniques, which is a passive technique is promising because, AE sensors can detect even a smallest leakage quickly, offering high sensitivity regarding fault growth in a pipeline system. Very few researchers have exploited AE-based techniques for pipeline diagnostics [2–8]. Lee et al. [9] used AE technique to detect pipeline leakage. Two different methods were used for determining source location, i.e., attenuation-based method and time of flight-based method. It was found that attenuation-based method was more effective to detect leaks. Gao et al. [10] determined the position of a leak in buried water distribution pipes by accurate estimation of the time delay between two measured acoustic signals. By using a model for the wave propagation along plastic pipes, various time delay estimators using cross-correlation were compared for their ability to locate a leak in plastic pipes. Kim et al. [11] identified the characteristics of dispersion of acoustic wave through analysis of the cut-off frequency by using the time–frequency method experimentally and theoretically for the development of an experimental tool to analyze the leak signals in steel pipe.

Ahadi et al. [12] proposed a method for capturing a leakage signal-signature in time domain by monitoring the Short Time Fourier Transforms (STFT) of AE signals over a relatively long time-interval. This captured signal was then used to fine tune wavelet for the best signal localization in time and frequency domains. The results of this experimental study shown that using tuned wavelet, AE events were detected and identified. Ozevin et al. [13] proposed a new leak localization approach for pipeline networks spread in a two-dimensional configuration using one dimensional source location algorithm. The attenuation and the wave velocity study with distance were integrated with the location for any kind of pipeline materials in order to increase the reliable leakage location. Khulief et al. [14] presented an experimental investigation that addressed the feasibility and potential of in-pipe acoustic measurements for leak detection. The acquired acoustic signals were analyzed and it was found that the relatively low frequencies associated with the unsteady flow separation at the leak point which is useful for leak detection. Wang et al. [15] presented an improved cross-correlation algorithm for high-precision pipeline leak detection based on wavelet transform and energy feature extraction. Both energy and frequency features of AE signals were taken into consideration to determine the time delay for leak location.

Juliano et al. [16] used acoustic emission method to detect leaks and discerned their location under flow conditions in a 304.8-m-long, 305-mm-diameter buried steel pipeline. A leak of 16.2 mL/s was successfully detected, and it's location was indicated to within 0.3 m. Lin et al. [17] proposed a non-intrusive detection method for gas pipeline leak based on piezoelectric acoustic sensors. The experimental results verified it's feasibility and effectiveness. Jin et al. [18] proposed an integrated model to detect and localize gas pipeline leakage. The model mainly contains pipeline leakage localization method, de-noising method for acoustic signals, and recognition method for acoustic signals under different work conditions. Putra et al. [19] investigated the relation between leak properties and acoustic emission signal. Wave attenuation constant β was obtained based on experimental result where the amplitude varies with the spatial and inside pressure of pipe. Mostafapour et al. [20] proposed a noble method for continuous leakage source location with one sensor in gas-filled steel pipe and noisy environment based on wavelet analysis and modal location theory. The leakage signals were analyzed into high and low frequencies by wavelet decomposition and noises and reflected waves were omitted. Xu et al. [21] proposed a novel leakage localization approach based on the multi-level framework. The approach consisted of two steps: regional localization and precise localization. The regional localization was to determine the region of the leakage source and then the precise localization results were obtained by the cross-correlation analysis.

Yu et al. [22] conducted an experimental investigation on AE based small leak detection of galvanized steel pipe due to screw thread loosening. The waveform, frequency and energy signatures of the AE signals were first extracted and compared. It was observed that four of the eight characteristic of the small leak signals showed a great difference compared with that of environmental noise: mean value, RMS value, peak frequency and energy. Pan et al. [23] proposed an acoustic emission sensor for collecting and analysing leakage signals inside the pipeline. Four operating conditions of a fluid-filled pipeline were established and a support vector machine (SVM) method was used to accurately classify the leakage condition of the pipeline. Ye et al. [24] analysed the AE mechanism and basic characteristics of valve leakage and then the theoretical relationship between standard deviation of AE signal of valve leakage and the leakage rate was determined. It was found that when the valve leakage is small, there is a linear relationship between the standard deviation of the AE signal and the leakage rate. Nicola et al. [25] developed a pipeline leak-off detection system based on the principle of leak location by means of the cross-correlation method. Quy et al. [26] proposed a reliable leak detection method for water pipelines under different operating conditions. This approach segments acoustic emission (AE) signals into short frames based on the Hanning window. An intermediate quantity, which contains the symptoms of a leak and keeps it's characteristic adequately stable even when the environmental conditions change, was calculated.

From the thorough literature review, it is observed that leakage detection in a pipeline system is a grey area. Also, even though number of studies are carried out on leakage detection, not much focus was given to apply AE for leakage in pipelines (with different flow rates). Hence, in this study, authors have focused on important AE parameters which are having influence with change in leakage rate of flow.

2.0 Experimental Study

Experimental study is carried out towards leakage detection in a pipeline using acoustic emission technique (AE). A steel pipe of 2000 mm length having internal dia. 254 mm and thickness of 5 mm is used. Seven wide band AE sensors are affixed linearly on the pipe at a distance of 250 mm from one end. For any type of health monitoring system, placement of sensors plays major role for obtaining important information about the structure. In this study, seven AE sensors are placed to get more accurate location of leakage. Surface of the pipe need to be cleaned before placing sensors. Special holders are fabricated and affixed on the specimen using the help of glue material and then AE sensors are mounted on the specimen. These AE sensors are affixed by applying coupling material (grease) to avoid air gap between sensor and specimen. Threshold and pre-amplifier gain is set as 40 dB. Threshold limit need to be set before starting the test to avoid environmental noise. Analog filter of 1 kHz to 400 kHz and sampling rate of 3 MSPS is used to detect the leakage in the pipe. Initially, pencil lead brake (PLB) test is carried out to check the sensitivity of AE sensors and wave velocity. PLB test is performed near sensor 1 (Fig. 4) and signals are received by sensors 1 and 2, the measurement AE response is shown in Fig. 3. Based on this test, wave velocity in the pipe

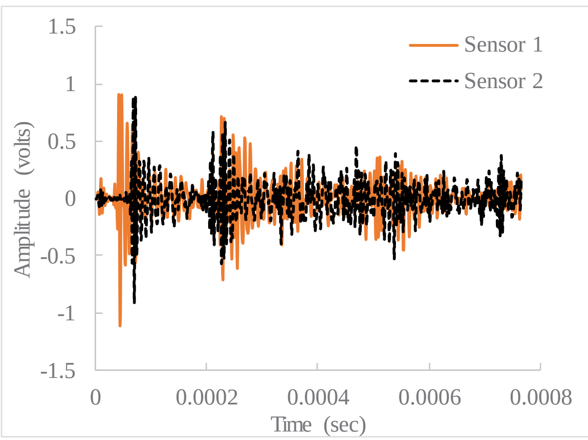

Figure 3 : Pencil lead break (PLB) test

is evaluated and given as input during AE testing of the pipe under leakage conditions.

Leakage in the pipe is simulated using a valve, manually opening and closing at different flow rate of leakage. Experimental setup of the study is shown in Fig. 4. Water is used as fluid in the pipeline and pressurised. Pressure in the pipe is monitored using pressure gauge. A constant pressure of 35 bar is applied and the valve is slowly released manually at different rate of flow through the valve (simulated leakage). Studies are carried out for different flow rates (leakage) of 200, 400, 800, 1600, 4800 ml/minutes. AE features are extracted from the measured responses by the sensors and further processed to assess leakage in the pipe.

3.0 Results and Discussion

3.1 AE Counts for localising leakage for different leakage flow rates

AE count refers to the number of pulses emitted by the measurement circuitry if the signal amplitude is greater than the threshold limit. Depending on the magnitude of the AE event and the characteristics of the material, one hit may produce one or many counts. AE energy is the measurement of the area under the envelope of the rectified linear voltage time signal captured by the transducer. Hence, recorded AE counts and AE energy data are processed to obtain meaningful results. AE counts and cumulative AE energy for all the sensors for the flow rate of 1600 ml/minutes are shown in Figs. 5(a) and (b) respectively. AE counts and cumulative energy plot show that leakage is happening nearer to the sensor 6 because highest counts and energy is released nearer to this sensor. It is observed that, leakage in the pipe is possible to localise using the AE parameters.

Further, data is processed to characterize leakage in the pipeline for different rate of flow of leakage. AE counts at different measurement locations under different leakage flow rate by sensor 1, sensor 4 and sensor 6 which are 1.25 m, 0.5 m and 0.1 m apart from leakage are shown in Fig. 6(a). Fig. 6(b) shows the slower leakage flow rate (200, 400 and 800 ml/minutes) versus AE counts. These plots show that using AE counts from higher flow rate to lower flow rate of leakage can be identified.

Figure 4 : Experimental setup for leakage detection

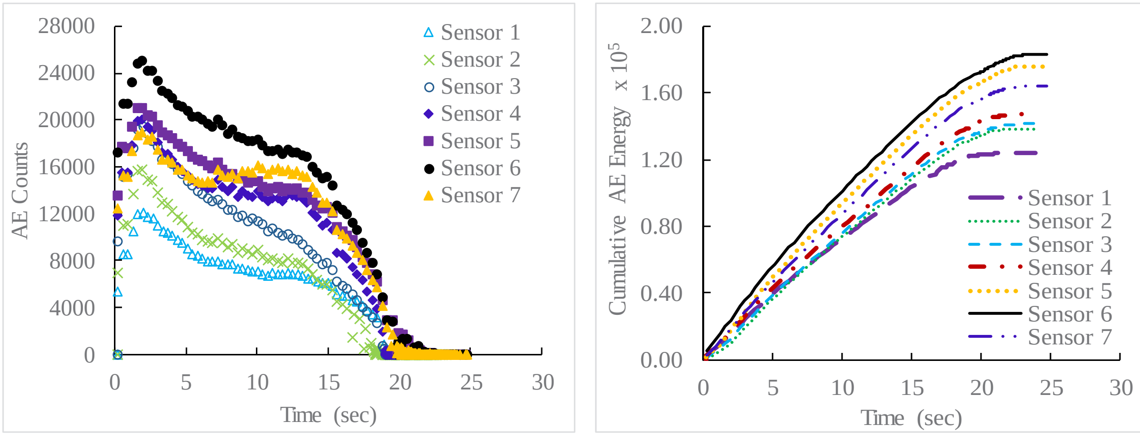

(a) (b)

Figure 5 : Time versus (a) AE counts and (b) Cumulative AE energy

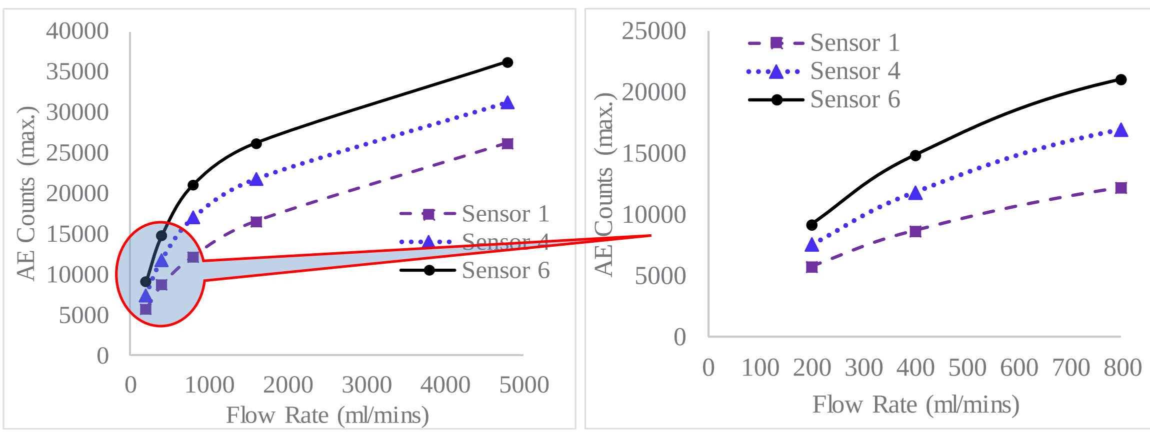

(a) For all the flow rate (b) for slow flow rate

Figure 6 : AE counts plots with respect to flow rate

3.2 *AE Energy for localising leakage for different leakage flow rates*

AE energy with respect to time for different flow rates for sensor 1, sensor 4 and sensor 6 is shown in Fig. 7. Fig. 7(a) shows the AE energy plot with respect to all the flow rates and Fig. 7(b) shows for the slow flow rate cases, viz., 200, 400 and 800 ml/minutes. From Figs. 7(a) and (b), it is stated that AE energy along with other AE features can efficiently be utilised to identify the location of leakage and can also be used to distinguish rate of flow of leakage.

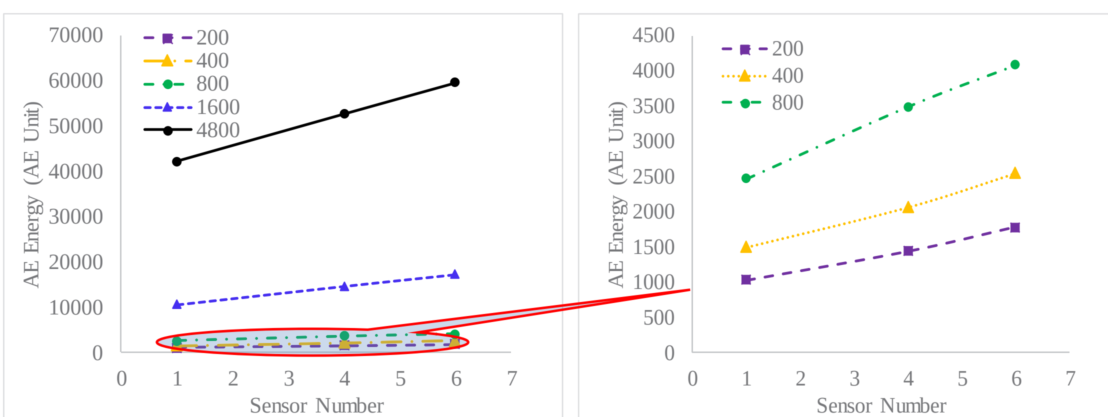

(a) For all the flow rate (b) for slow flow rate

Figuer 7 : AE energy plots with respect to flow rate

3.3 *Signal Strength for localising leakage for different leakage flow rates*

Acoustic emission signal strength is defined as the measured area of the rectified AE signal with units proportional to volt-seconds. Signal strength normally includes the absolute area of the positive and negative envelopes. Hence, signal strength can be used to relate leakage in the pipeline. Hence, in this study, signal strength data is captured and processed to identify leakage in the pipe under different rate of flow of leakage. Fig. 8(a) shows signal strength with respect to different flow rates and Fig. 8(b) shows the signal strength with respect to slow flow rate. It can be observed that, using signal strength data also, leakage location can be identified.

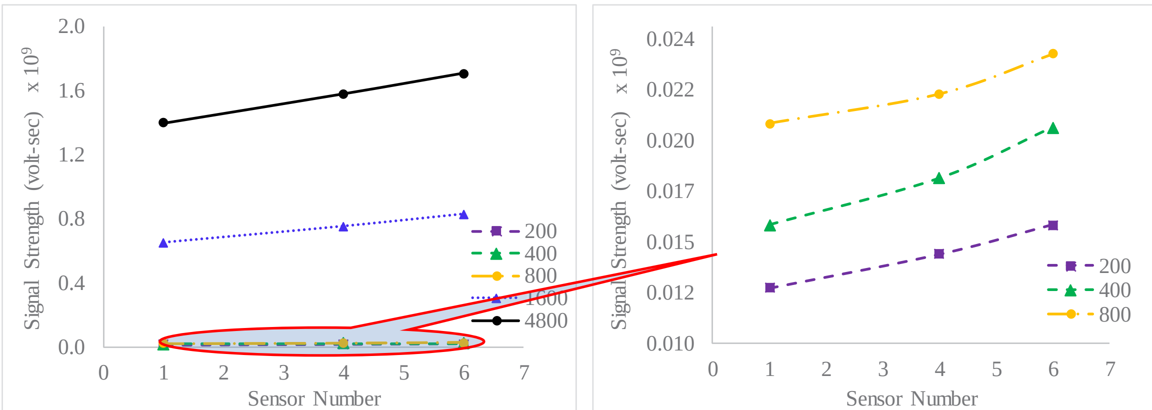

(a) For all the flow rates (b) for slow flow rate

Figure 8 : AE signal strength with respect to different flow rate

3.4 *Standard Deviation for localising leakage for different leakage flow rates*

AE hits data with respect to flow rate of 4800 ml/minute is processed. During the test, twenty numbers of AE hits are captured by all the AE sensors. Further, AE hit signal waveform is processed to obtain standard deviation of sensor 1 to 6 with respect to flow rate 4800 ml/minute is evaluated as shown in Fig. 9 and it is found that using standard deviation also, leakage location can be identified.

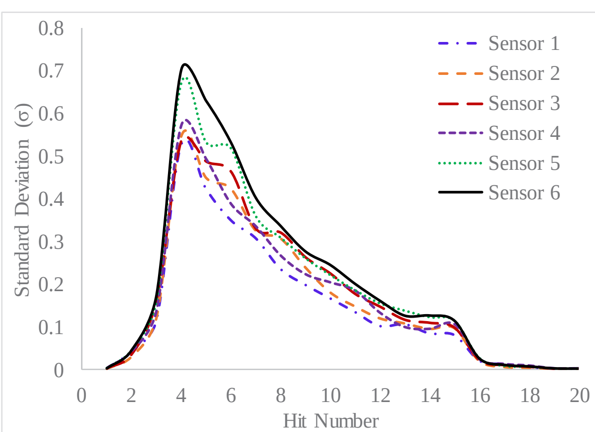

Figure 9 : Standard deviation with respect to leakage flow rate of 4800 ml/minutes

4.0 Conclusions

In the present study, experimental investigations carried out for leakage detection in the pipeline using acoustic emission technique for different flow rate of leakage is discussed. From the studies, the following observations are made.

i) It is found that the AE features could be used to localize the leakage in the pipeline.

ii) The acoustic features such as AE counts, AE energy, and signal strength are observed to be important AE parameters. The results from the experiments show that the AE parameters are very effective in localising leakage in the pipeline.

iii) Also, the influence of leakage flow rate is studied and it is found that AE features can distinguish the rate of leakage whether minor or major.

iv) The present study showed the effectiveness of utilising acoustic emission technique to identify and localize the leakage in the pipeline as well as to qualitatively assess the rate of leakage.

This study is limited to short length of pipelines under laboratory conditions, and further studies are needed to be carried out for further establishing the AE technique for real service conditions on prototype pipeline systems.

References

1. Rens, K. L., Wipf, T. J., Klaiber, F. W.: Review of Nondestructive Evaluation Techniques of Civil Infrastructure. Journal of Performance of Constructed Facilities 11(4), 152-160 (1997).

2. Mandal, S. K., Chan, F. T. S., Tiwari, M. K.: Leak detection of pipeline: An integrated approach of rough set theory and artificial bee colony trained SVM. Expert Syst. Appl. 39, 3071-3080 (2012).

3. Sun, J., Wen, J.: Target location method for pipeline pre-warning system based on HHT and time difference of arrival. Measurement 46, 2716–2725 (2013).

4. Xiao, Q., Li, J., Bai, Z., Sun, J., Zhou, N., Zeng, Z.: A Small Leak Detection Method Based on VMD Adaptive De-Noising and Ambiguity Correlation Classification Intended for Natural Gas Pipelines. Sensors 16, 2116 (2016).

5. Martini, A., Troncossi, M., Rivola, A.: Leak Detection in Water-Filled Small-Diameter Polyethylene Pipes by Means of Acoustic Emission Measurements. Appl. Sci. 7(1), 1-13 (2016).

6. Martini, A., Troncossi, M., Rivola, A.: Vibroacoustic Measurements for Detecting Water Leaks in Buried Small-Diameter Plastic Pipes. J. Pipeline Syst. Eng. Pract. 8(4), 04017022 (2017).

7. Li, S., Song, Y., Zhou, G.: Leak detection of water distribution pipeline subject to failure of socket joint based on acoustic emission and pattern recognition. Measurement 115, 39-44 (2018).

8. Nicola, M., Nicola, C. I., Vintila, A., Hurezeanu, I., Duta, M.: Cross-Correlation, Acoustic emission, Leakage detection, LabVIEW environment. J. Mech. Eng. Autom. 8, 59-67 (2018).

9. Lee, M-R., Lee, J-H.: Acoustic emission technique for pipeline leak detection. Key Engineering Materials Vols. doi:10.402/KEM.183-187.887 (2000).

10. Gao, Y., Brennan, M. J. Joseph, P. F.: A comparison of time delay estimators for the detection of leak noise signals in plastic water distribution pipes. Journal of Sound and Vibration 292(3-5), 552-570 (2006).

11. Kim M-S., Lee, S-K.: Detection of leak acoustic signal in buried gas pipe based on the time–frequency analysis. Journal of Loss Prevention in the Process Industries 22(6), 990-994 (2009).

12. Ahadi, M., Bakhtiar, M.S.: Leak detection in water-filled plastic pipes through the application of tuned wavelet transforms to Acoustic Emission signals. Applied Acoustics 71(7), 634-639 (2010).

13. Ozevin D., Harding, J.: Novel leak localization in pressurized pipeline networks using acoustic emission and geometric connectivity. International Journal of Pressure Vessels and Piping 92, 63-69 (2012).

14. Khulief, Y. A., Khalifa, A., Mansour, R. B., Habib, M. A.: Acoustic detection of leaks in water pipelines using measurements inside pipe. Journal of Pipeline Systems Engineering and Practice 3, 47-54 (2012).

15. Wang, X., Zhao, M., Li, S.: An improved cross-correlation algorithm based on wavelet transform and energy feature extraction for pipeline leak detection. International Conference on Pipelines and Trenchless Technology (ICPTT 2012), China (2012).

16. Juliano, T. M., Meegoda, J. N., Watts, D. J.: Acoustic emission leak detection on a metal pipeline buried in sandy soil. Journal of Pipeline Systems Engineering and Practice ASCE 4(3), 149-155 (2013).

17. Lin, W., Jiang, L., Wu, H.: Study of non-intrusive gas pipeline leak detection with acoustic sensor. 3rd IFAC International Conference on Intelligent Control and Automation Science, China (2013). doi:10.3182/20130902-3-CN-3020.00039.

18. Jin, H., Zhang, L., Liang, W., Ding, Q.: Integrated leakage detection and localization model for gas pipelines based on the acoustic wave method. Journal of Loss Prevention in the Process Industries 27, 74-88 (2014).

19. Putra, I. B. A., Prasetiyo, I., Sari, D. P.: The use of acoustic emission for leak detection in steel pipes. Applied Mechanics and Materials 771, 88-91(2015).

20. Mostafapour, A., Davoodi, S.: Continuous leakage location in noisy environment using modal and wavelet analysis with one AE sensor. Ultrasonics 62, 305-311 (2015).

21. Xu, C., Gong, P., Xie, J., Shi, H., Chen, G., Song, G.: An acoustic emission based multi-level approach to buried gas pipeline leakage localization. Journal of Loss Prevention in the Process Industries 44, 397-404 (2016).

22. Yu, L., Li, S. Z.: Acoustic emission (AE) based small leak detection of galvanized steel pipe due to loosening of screw thread connection. Journal of Applied Acoustics 102, 85-89 (2017).

23. Pan, S., Xu, Z., Li, D., Lu, D.: Research on detection and location of fluid-filled pipeline leakage based on acoustic emission technology. Sensors 18(11), 3628 (2018). doi:10.3390/s18113628.

24. Ye, G-Y., Xu, K-J., Wu, W-K.: Standard deviation based acoustic emission signal analysis for detecting valve internal leakage. Sensors and amp; Actuators: A. Physical. 283, 340-347 (2018).

25. Nicola, M., Nicola, C-I., Vintila, A., Hurezeanu, I., Duta, M.: Pipeline leakage detection by means of acoustic emission technique using cross-correlation function. Journal of Mechanical Engineering and Automation 8(2), 59-67 (2018). doi: 10.5923/j.jmea.20180802.03.

26. Quy, T. B., Muhammad, S., Kim, J-M.: A reliable acoustic emission-based technique for the detection of a small leak in a pipeline system. Energies 12, 1472 (2019). doi:10.3390/en12081472.

Failure Analysis of Attemperator Nozzle in Heat Recovery Steam Generator Units

Ayush Gangwar[1], Manindra Pratap Singh[2], Mayank Banjare[3], and B.K.Muduli[4]
[1] Panipat Naphtha Cracker, Indian Oil Corporation Ltd, Panipat, India.
[1]gangwara2@indianoil.in
[2] Panipat Naphtha Cracker, Indian Oil Corporation Ltd, Panipat, India
[2]singhmanindra@indianoil.in
[3] Panipat Naphtha Cracker, Indian Oil Corporation Ltd, Panipat, India
[3]banjaremayank@indianoil.in
[4] Panipat Naphtha Cracker, Indian Oil Corporation Ltd, Panipat, India
[4]mudulibk@indianoil.in

ABSTRACT

Superheated steam (SHP steam) plays a crucial role in the power generation facility/industry. Significant potential lies in its ability to store an incredible quantity of internal energy that is utilized as a source of kinetic energy through expansion against the turbine blade in steam turbines. The generation of SHP steam requires additional heat input after evaporation to further heat it above its saturation temperature.

Precise management of steam temperature is a critical element for safe and economical plant operation. In HRSGs, to maintain the required SHP steam temperature and pressure a special type of desuperheater plays a vital role. Rapidly varying load conditions throughout regular operations and frequent startups-shutdowns are typical for HRSG. Depending on the boiler operating characteristics and the extent of load change, the attemperator can experience high stress. Close monitoring of various operational parameters (such as the temperature of superheated steam requires desuperheating, set temperature to attain final SHP steam temperature and pressure and operation of control valve regulating Injectant flow to control superheat) at different steam load conditions is necessary to avoid untimely failures of the desuperheating system.

The subject paper briefly discusses the assorted operational scenario and metallurgical factors that led to a typical failure of the desuperheating water spray nozzle. Elaborated analysis for the failure has been discussed within the paper along with adopted counter- measures to mitigate similar failures in the future.

Keywords: HRSG, Desuperheater, Temperature control, Spray Nozzle

Introduction

The failure of an attemperator desuperheater in Heat Recovery Steam Generator (HRSG) has been investigated. There are five HRSG's in Panipat Naphtha Cracker producing 96 TPH of superheated steam at 525^0C @ 125 kg/cm^2 of pressure. These parameter results in a 200^0 of superheat in steam with respect to the saturation steam produced at the same pressure.

Superheated steam can't be generated in the evaporator section of the boiler alone, due to thermodynamic equilibrium as any additional heat simply evaporates more water and the steam will become saturated steam. To generate the SHP steam, equilibrium is violated temporarily in a High-Pressure boiler by drawing saturated steam from the evaporator section through a steam drum and passing it through a separate heating section of superheaters, which transfers additional heat to the steam.

Precise control of steam temperature is a critical element for safe and efficient plant operation, which is achieved through an attemperator type de-superheater installed between two superheaters (SH) panels SH-5 and SH-4 in HRSG as shown in figure (Figure-1). Desuperheater regulates steam temperature by injecting (Boiler Feed Water) BFW into the steam flow within the SHP steam boiler circuit. This direct contact between the SHP steam and atomized BFW causes evaporation, resulting in a decrease in steam temperature.

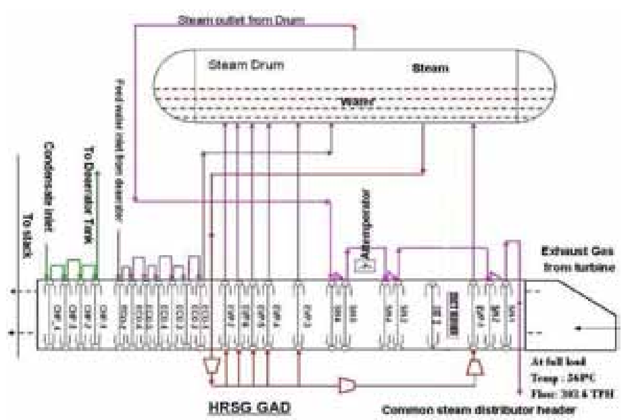

Figure 1 : HRSG-GAD

Materials and Methods

Visual and DPT Observations

Cracks were observed in the injection nozzle of all HRSG's. The origin of cracks was the main injection hole provided on the internal side of the nozzle. Complete dislodgment of the nozzle due to weld failure was observed in HRSG-4.

Table 1: Visual & Dot Observation in HRSG'S

Sr. No.	Unit	Visual and DPT Observation	Image
1	HRSG-1	A total of three cracks were observed in the nozzle, out of those three two major cracks were observed to be extended from nozzle face into its body	
2	HRSG-2	A fine crack was observed in the internal face of the nozzle. The crack seems to be originated from the injection piping and extended in the nozzle body	
3	HRSG-3	Crack was observed in the outer surface of the diverging section of desuperheater DSH nozzle	
4	HRSG-4	DSH nozzle at spray end of desuperheater was found dislodged	
5	HRSG-5	A wide through n through crack was observed in the lower section of at 6'o clock position in the injection nozzle	

Microstructural Examinations

For further inspection of cracks in nozzles of attemperator, the help of in-situ metallographic inspection was taken (Figure-7). In-situ metallographic was carried out at two spots on the attemperator nozzle. The first spot was taken on the base metal of the nozzle and second was over crack surface. Surface preparation was carried as per the standard procedure. The polishing of the sample surface was carried out with diamond slurry before etching. The etching was done using waterless Kalling's etchant ($CuCl_2$=5 grams, Hydrochloric acid=100 ml and Ethanol=100 ml). Replica of the surface was taken on cellulose acetate film and further examination was carried out in an optical microscope and scanning electron microscope.

Figure 2 : Surface ptreparation, Etching And Replica Generation for DSH Nozzle for in-situ Metallography

Kalling's etchant mainly attacks the ferritic and martensitic phases. In microstructure darkest phase will be ferrite, martensite will be darker and austenite will be light.

Results and Discussion

Visual observation of failed attemperator revealed the branched cracks in welds and parent metal of nozzle. These types of cracks are the result of stress generated due to expansion and contraction experienced by nozzle subjected to heating and cooling cycles.

Microstructure analysis revealed a matrix of an austenitic matrix with annealing twined grains. No material degradation was observed in base metal (Figure-8).

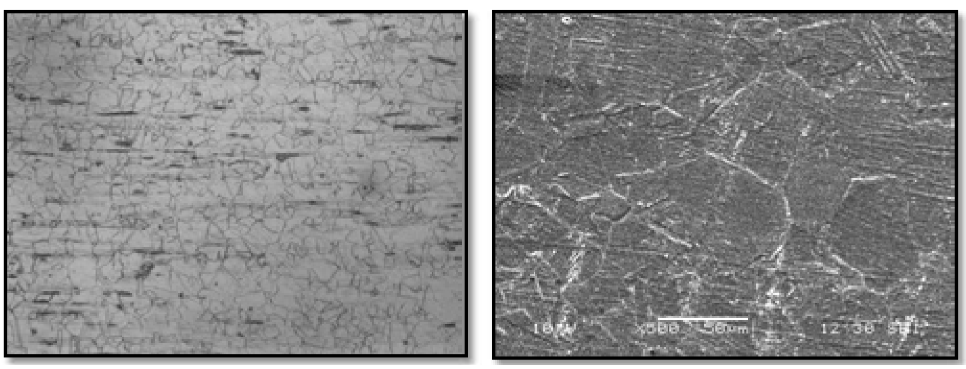

Figure 3 : Matrix's Microstructure at 200X and 500X of DSH Nozzle

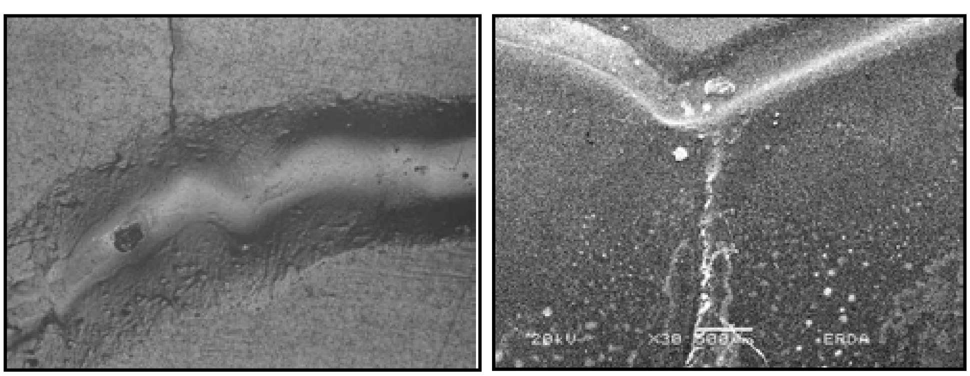

Figure 4 : Microstructure of Crack at 200X and 500X in DSH Nozzle

No material degradation was observed in the periphery of crack. Crack nature was trans-granular and observed to be propagating in a straight line (Figure-8).

On examining microstructures from the sample it was revealed the no material degradation occurred in the matrix and regions near the crack. The nature of crack also appeared to be trans-granular and propagating in a straight line. As no degradation of the material was observed, the crack may have originated due to some thermo-mechanical impact, like thermal/mechanical shock, vibrations or thermal cyclic stress resulting in thermal / fatigue cracking.

For further analysis of failure trends of the operational parameter was analyzed for various situations like startup, normal operations and shutdowns. Opening and Closing of the BFW flow control valve is controlled by the temperature difference in the receiving stream i.e. output steam from SHP Panel-4 and set pressure. Higher the temperature difference, the larger opening of a control valve, therefore heavier dumping of BFW for cooling.

The irregular operation causes frequent fluctuations in the temperature of output steam from SHP Panel-4.

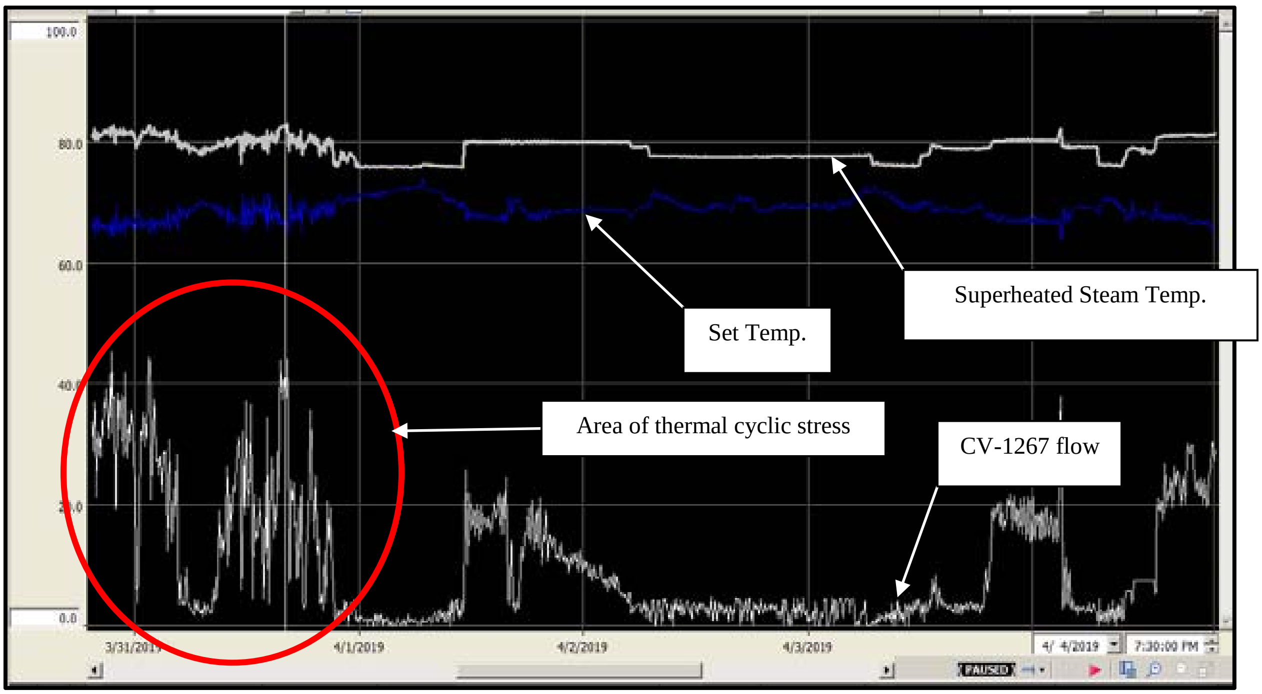

Figure 5 : Thermal Cyclic Stress in Attemperator Nozzle

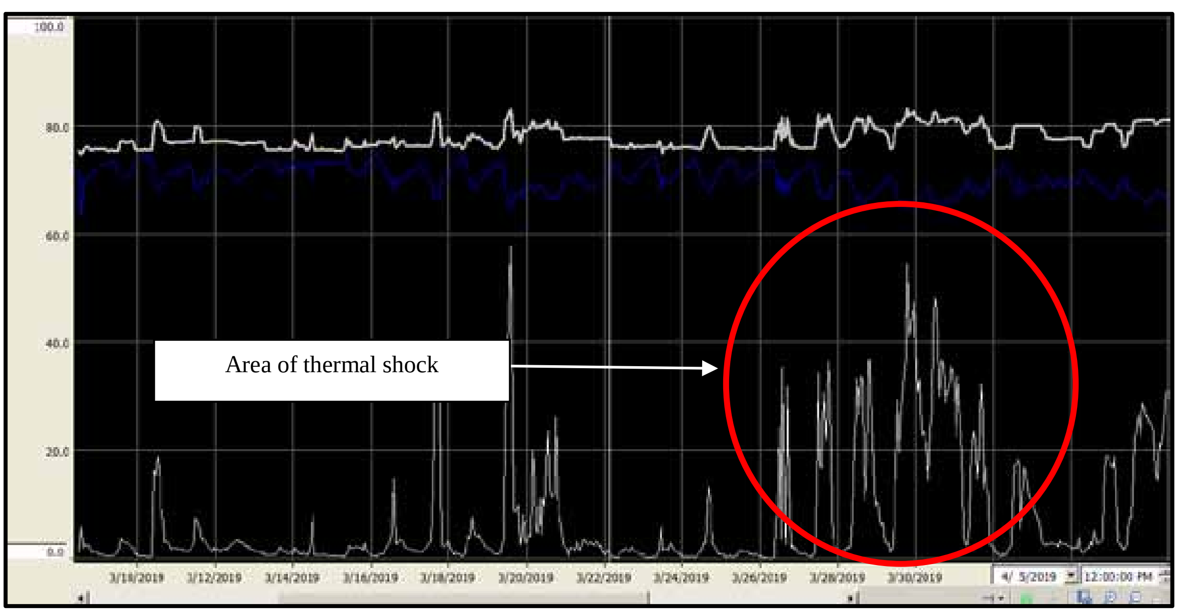

Figure 6 : Thermal Shock in Attemperator Nozzle

To obtain an optimum temperature in the outlet of desuperheater continuously, the BFW flow control valve has to vary its opening to match the temperature fluctuations. Continuous operation of the attemperator control valve in a variable manner results in thermal cyclic stress on the attemperator nozzle.

Very large temperature difference in the superheated steam temperature in the upstream section of desuperheater and de-superheated steam in the downstream section of desuperheater results in the immediate opening of BFW flow control valve has to dump a huge amount of BFW to desuperheat. A large opening in an instantaneous manner results in thermal shock in the desuperheater nozzle.

Rapidly varying load conditions are typical in the regular operation of HRSG's, depending on the boiler operating characteristics and the extent of load changes attemperator can experience extensive thermal cycling & thermal shock. Various factors like high ΔT between the receiving steam i.e. SHP steam and injecting steam i.e. BFW, intermittent desuperheater operation, low-load boiler operation, frequent startups & shutdown of the boiler may contribute to attemperator failures.

Conclusions

During operation injecting stream i.e., BFW injected at 133°C and 185 kg/cm2 of pressure in the receiving stream of SHP steam at 450°C and 135 kg/cm2 of pressure. There exists a large ΔT of 317 °C between injecting at the receiving stream. This large value of ΔT results in thermal cyclic stresses due to variations of temperature.

No material degradation, ΔT>93°C & damage is in the form of cracking in an attemperator nozzle, where relative movement or differential expansion is constrained, particularly under repeated thermal cycling gives the indication that failure might have occurred because of thermal fatigue.

References

[1] Goutam Mukhopadhyay and Sandip Bhattacharyya (2011) "Failure analysis of an attemperator in a steam line of a boiler", Engineering Failure Analysis 18 (2011) 1359–1365.

[2] Schutte & Koerting Process Products & Systems (2012) "Desuperheater Manual Revision-3"

[3] Kristin Donahue, Graham Corporation (2001) "Desuperheater Selection and Optimization", Chemical Engineering, August 2001 Chemical Week Associates, L.L.C.

[4] Scott A Wambeke, PE, HRST Inc (2004) "Avoid desuperheater problems with quality equipment, proper installation, tight process control", COMBINED CYCLE JOURNAL, Fourth Quarter 2004

Phased array ultrasonic inspection of dissimilar weld joints in nuclear facility by experiment and simulation

S.Kumar[1*], M.Menaka[2], B.Venkatraman[1,2]
[1]Homi Bhabha National Institute, Indira Gandhi Centre for Atomic Research, Kalpakkam, 603109, India
[2]Radiological & Environmental Safety Division, Indira Gandhi Centre for Atomic Research, Kalpakkam, 603109, India
*skumarqad@igcar.gov.in

ABSTRACT

Dissimilar metal welds (DMWs) between the main vessel pipeline and steam generators joints in nuclear power plants are commonly inspected by Phased array ultrasonic testing (PAUT). The occurrence of beam splitting and skewing in the ultrasonic inspection will affect the defect detection, localization and sizing of the defect. This paper presents the study on phased array ultrasonic method for evaluation of dissimilar welds using advanced probes such as linear array probes and dual matrix array probes. In the present study, a simulation is performed for understanding the ultrasonic beam propagation and improving the defect detectability in DMWs by a combined approach of the ray-based model and semi- analytical model. Experiments are carried out in P91 to Alloy 800 weld plates (12 mm thick plate with defects) using 16 x 2 DMA probes at 4 MHz frequency and 16 elements linear array probe at 5 MHz with 55 Shear wave & 60 Longitudinal wave wedges. Simulated results of the defect detection in the welds were validated with experimental results. The result of the simulation as well as experiments shows the dual matrix array probe gives the better defect detectability and beam propagation into the welds. The DMA probes eliminate the interface echo, dead zones due to wedge echoes & reduces the backscattering signals, thus improving the flaw detection and sizing of dissimilar welds by combining the benefits of low frequency longitudinal focused beam and transmit- receive inspection technique.

Keywords: Dissimilar welds, Simulation, Linear array probe, Dual matrix array probe.

1. Introduction

In Prototype Fast Breeder Reactor (PFBR), Dissimilar welds fabricated between the main structural and piping material (austenitic SS 316LN) and the steam generator material (Modified 9Cr-1Mo steel (P91)) [1,2]. Alloy 800 is a intermediate piece connected between the 316L(N) SS and P91 steel to reduce the thermal stress during operation. Ultrasonic techniques (UT) are extensively used during in-service inspections of components in nuclear power plants, because of their capabilities to detect and size potential in-depth flaws [3]. The inspection of dissimilar weld components is complicated because of anisotropic and inhomogeneous properties of the welding materials leading to beam splitting and skewing which affects the detection, localization and sizing of weld discontinuities [4]. Phased array ultrasonic techniques (PAUT) offer significant technical advantages for weld inspections over conventional ultrasonic because of the beam steering, scanning and focusing capabilities. Beam steering allows ultrasonically optimization of the selected beam angles and orienting into perpendicular to the predicted defects.

Analyzing the processes of ultrasonic propagation and scattering that arise in a weld is a challenging case study for several theoretical and numerical aspects this is because the elastic properties of weld materials are anisotropic and heterogeneous which occurs due to the grain growth during the solidification process and succession of welding layers deposition [5]. However, the use of phased array ultrasonic tests for Dissimilar Metal Welds (DMW) inspection is difficult due to misrepresentation of weld material and inappropriate focal laws for focusing and/or steering ultrasonic beams at the desired position through anisotropic and inhomogeneous medium [6]. Simulation is a very useful tool in understanding the results of inspection and the complex phenomena viz., anisotropic and heterogeneous. Simulation tool helps to optimize ultrasonic NDT and plays an important role in developing advanced reliable UT techniques. It also helps in optimizing experimental parameters for inspecting dissimilar weld components and it is used for quantitative prediction of inspection parameters.

The ATHENA 3D finite element (FE) model developed by EDF (Electricite de France) R&D helps in the study of wave propagation in DMW media from the 2D model. This model developed to predict the effect of propagation and scattering of surface waves from the surface defects and complex geometry [7]. The pencil method was developed as an extension of the Deschamps formula to predict elastodynamic fields in anisotropic and heterogeneous components radiated by elementary sources [9]. Later a method was developed for field computation by the French Atomic Energy Commission (CEA) which is based on the propagation of pencils, since this approach provides both numerical efficiency and accuracy and is able to deal with complex configurations [11]. The whole inspection (prediction of scattered echoes received by the probe for each scanning position) can be simulated using an argument based on the Auld's reciprocity theorem of the incident field and the defect scattered echoes [8]. This approach has led us to develop approximate models for the various phenomena involved in ultrasonic inspections viz., radiation, interface transmission, propagation, defect, physical boundary scattering and reception, etc. [10]. The beam propagation and defect response are calculated using semi-analytical formulations and dynamic ray tracing model which is used in CIVA software developed by CEA [12-14]. These models are capable of predicting and compensating for beam distortions or deviations in a complex and/or anisotropic specimen [15]. Using phased array simulation, optimization of the inspection condition and increasing the signal-to-noise ratio for dissimilar metal welds tests can be done. Inspection results with the flexible phase array combined with CIVA's reconstruction functionality shows the ability to locate and accurately size flaws under a complex 3D geometry component [16].

In this paper, the phased array ultrasonic testing of DMWs is investigated by simulation and experiment. Two different types of probes (linear array (LA) with (shear wave (SW) & longitudinal wave (LW)) & dual matrix array (DMA)) with longitudinal wave (LW) are investigated by phased array ultrasonic testing of DMW. Two welded specimens are prepared by Gas Tungsten Arc Welding (GTAW) process. The DMW specimen will be examined for their microstructure which includes grain size distribution. Ultrasonic modelling software tool (CIVA) is used to predict the ultrasound propagation in the DMW. CIVA model is applied to a weld which is described using a constant which in turn consists of a set of several domains.

Simulation of ultrasonic inspection

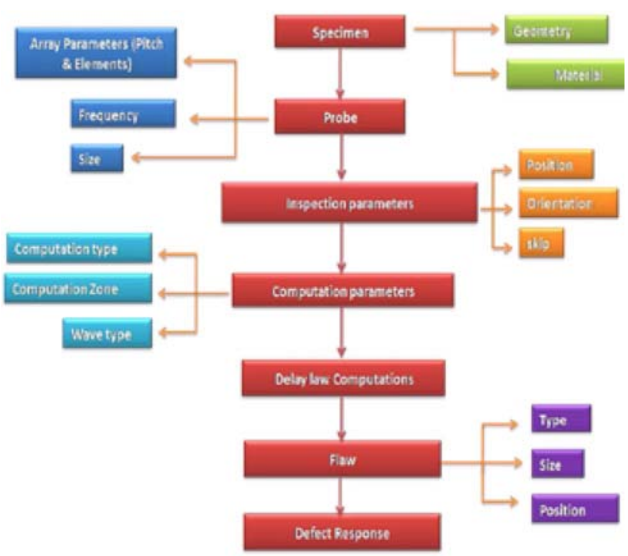

Figure 1 : Flow chart for simulation of ultrasonic inspection

The CIVA model is used as the primary platform for developing, testing and optimizing strategies to overcome the distortion of dissimilar welds. Semi-analytical codes for modeling ultrasonic wave propagation and interactions with discontinuities in anisotropic media are cost-effective for industrial parametric studies compared to computational and time-intensive finite element or difference codes. Simulation is important for understanding the physics of the inspection process, to study the feasibility of an inspection method or inspection areas or to optimize inspection parameters, for better interpretation of experimental results and to quantify the detection probability. CIVA 2015 (11.1) software developed by CEA was used to model the phased array ultrasonic inspection for simulation studies. The CIVA software uses bulk wave beam field predictions based on elastodynamics pencil method and defect response predictions based on Kirchhoff, GTD or Born models for beam/defect interaction [17,18]. The simulation flow chart is mapped in Figure 1.

Components which need to be inspected along with the required defect response predictions should be created as two-dimensional profile in the computer-aided-design (CAD) facility. After creating the two-dimensional profile, the three-dimensional solid model is subsequently extruded. After the three-dimensional solid model has been imported into CIVA, either beam computation or defect response option has to be selected. All sides of the CAD model are color coded as front, back, side and interface so that the ultrasonic probe can be properly attached. Two base metal zones and one weld zone are the three zones shown in the two-dimensional profile and appropriate ultrasonic velocity is assigned to each. The CIVA software has user interface screens to describe the characteristics and geometry of the transducer crystal element, phased array crystal assembly and parameters of inspection/ scan. It also describes wedge material and geometry, test sample material and geometry, geometry of the flaw type, and parameters of computation [19].

Experimental Methods

Modeling Parameters

The simulation was performed for inspection of weldments using linear array probe and Dual matrix array probe. The phased array probes consist of a transducer at the top of a wedge. Rexolite plastic with an angle of incidence 39° is made in the wedge. The transducer consists of a linear array type of 16 elements with a flat focus of 5 MHz. The width of the element is 0.6 mm and the gap between the elements is 0.04 mm. Sectorial scan with the inspection range of 40° to 70° for shear wave and 45° to 75° for longitudinal wave is adopted for simulation. DMA probe consists of 2 matrices of 32 elements (16 x 2) mounted on a 55° LW wedge. For this sectorial scan with the inspection range of 30° to 82° is used.

One set of parameters have been found in the literature and shown in the table 3 [20]. P91 and Alloy 800 base material is assumed to be isotropic and homogenous. The weld zone is assumed to be an anisotropic and inhomogeneous structure. These aspects are responsible for splitting and skewing the ultrasonic beam along its propagation. Longitudinal wave velocity is 5900 and 5700 m/s while shear wave velocity is 3230 and 2300 m/s for P91 material and Alloy 800 respectively which are used in the simulation. The model parameters selected matches very well with actual experimental parameters.

	C_{11}	C_{22}	C_{33}	C_{12}	C_{23}	C_{31}	C_{44}	C_{55}	C_{66}
GTAW	255.8	255.8	236	135.4	137.9	130.5	111.4	111.9	81.4

Table 3: Elastic constants of welding material

Material Details

The present study involves two welding samples in flat position of P91 steel and Alloy 800. The welds are fabricated with Inconel 82 (ENiCr-3) SFA 5.11 using Gas Tungsten Arc Welding process. Table 1 & 2 shows the chemical composition of P91 and Alloy 800. The thickness of base material, root face and root gap are 12 mm, 1 mm, and 2 mm, respectively. The dimensions of the welded samples are 200mm X 150mm X 12mm as indicated in figure 2. Each weld is machined with an artificial flaw by electro-discharge machining (EDM) process. Side Drill Hole (SDH) of diameter 2mm and 25mm length were machined at a depth of 6mm from the top surface of the weld. 2 notches having dimension of 15mm X 1mm are machined on the weld face with a depth of 1mm at various locations. Figure 2 also shows the artificial defects of SDH and Notches in dissimilar weld sample for calibration purpose. The probe scanning side (Alloy 800 as well as P91) is also additionally marked in the figure 2.

Microstructure Examinations

The microstructural features are characterized using metallographic specimens which are cut from the weld cross sectional areas. Metallographic specimens are grounded on wet SiC

paper with varying grain sizes viz,. 220, 400, 600, 800, 1000, 1200 & 2000 and degreased with acetone. These are rinsed with distilled water and dried in dry air, according to ASTM E3. Later these samples were polished through 3-5 μm diamond paste after which final polishing was done with 1-2 μm. P91 and alloy 800 are etched using Nital etchant (10ml nitric acid + 100ml ethanol) and Kalling etchant (5gm $CuCl_2$+ 100ml HCL+ 100ml Ethanol) respectively. The typical microstructures were observed from the base metal, weld metal and heat affected zone using optical microscopy.

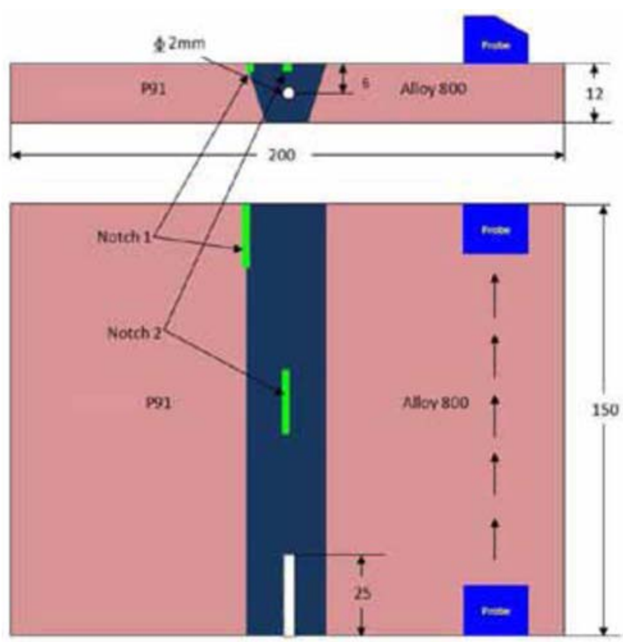

Figure 2 : Schematic diagram of weld joint configuration with Side drill hole and Notches

C	Cr	Ni	Mo	Mn	P	S	Si	Fe
0.082	8.39	0.39	0.87	0.38	0.008	0.001	0.26	Bal

Table 1 : Chemical composition of the P91 material (% in weight)

C	Cr	Ni	Cu	Mn	P	S	Ti	Fe
0.075	19.159	30.56	0.62	1.17	0.01	0.002	0.54	Bal

Table 2 : Chemical composition of the Alloy 800 material (% in weight)

Ultrasonic Examinations

Ultrasonic testing was performed using the omniscan MX2 and SX Olympus PAUT. The SA10-N55S&SA10-N60L wedges are used with the 5L16-A10 linear array probe and SA27-DN55L & SA27-DNCR wedges are used with the 5DM 16X2-A27 dual matrix probe for the DMW test. The ultrasonic longitudinal wave velocity is 5900 and 5700 m/s while shear wave velocity is 3230 and 2300 m/s for P91 material and Alloy 800 respectively. The values are obtained from the literature.

Radiography

All weld joints are examined using radiographic testing with a single wall single image technique to characterize artificial flaws and additional flaws. A model (Balteau 160 kV) of X-ray generator was used as the radiation source. A medium speed of fine grain (Agfa D4) film is used. Wire type penetrameters ranging from 250 microns to 810 microns with wire diameters were used. The penetrameter with step number 20 and with hole diameters 4T, 2T and 1T are also used. The penetrameters are placed on the source side.

Results and Discussion

Modelling results

Phased array ultrasonic simulation is performed by using a linear array probe (shear wave and longitudinal wave) and dual matrix array probe (longitudinal wave) with a half-skip path in the dissimilar weld. 2D cad profile of dissimilar weld is shown in figure 4. The probes are positioned at 10 mm from the weld centre (front of the wedge) in order to cover the root volume of the weld region. This surface distance is optimized for the LA probes and DMA probes for ultrasonic inspection of

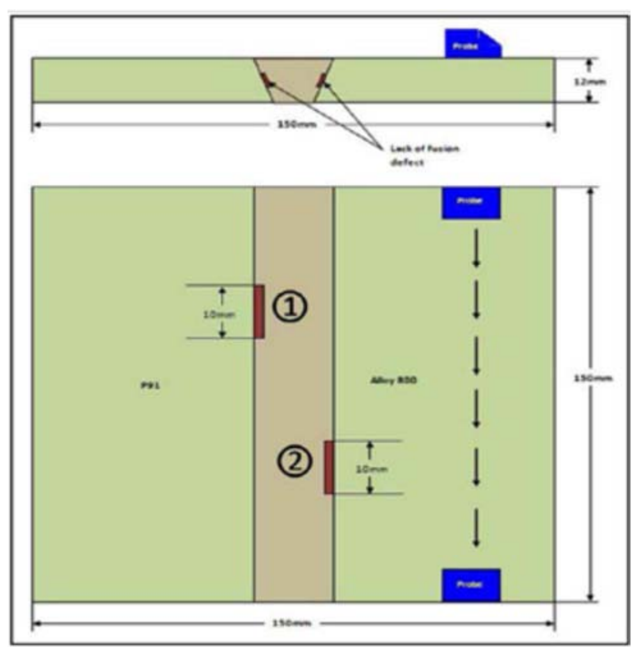

Figure 4 : 2D cad profile of dissimilar weld sample for simulation

dissimilar welds. For LA probe the sectorial scan is optimized for the range of 40° - 70° of the shear wave and for the range of 45° - 75° of the longitudinal wave respectively. For DMA probe, the sectorial scan with the range 30°- 82° is optimized.

The phased array ultrasonic generates a group of delayed waves, controlled by the focal law, which propagates a maximized wave front into the weld metal. The entire weld length has been scanned by moving the probes parallel to the weld length. The B-scan images are shown in figure 5,6&7 which represents the phased array results of linear array probe (shear wave), linear array probe (longitudinal wave) and DMA probe (longitudinal wave) respectively. In the B-scan image, the time-of-flight (travel time) or depth of the sound energy is displayed along the vertical axis and the linear position of the transducer is displayed along the horizontal axis. In the B scan image, one strong echo generated from the defect corner. Second, diffraction echo is generated from the tip of defect. Although multiple reflections from the weld microstructure observed in the experimental results are not taken into account in the simulation. The good correlation is achieved between the simulation and experimental for defect detection. During the scanning using shear wave, the greater the material attenuation, the greater the gain added to the signal should be allowed for defect detection. While Longitudinal wave, less attenuation due to the wavelength. DMA probe give better defect detection compared to LA probe due its pseudo focusing effect and separate transmitter and receiver. From the table 4, it is evident that the DMA probe with longitudinal wave gives better defect detection response and it is better for investigation of dissimilar welds inspection.

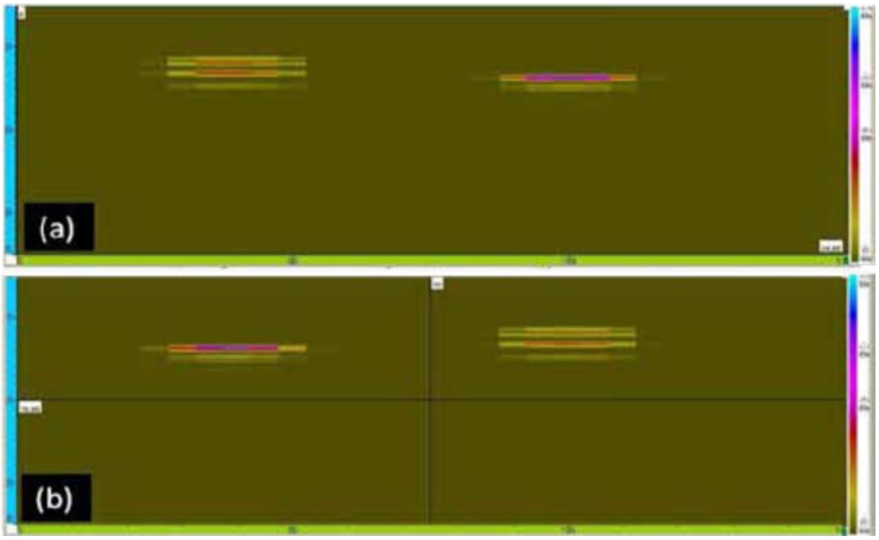

Figure 5 : Simulated B Scan images of LA probe (SW) scanned from (a) P91 side and (b) Alloy 800 side

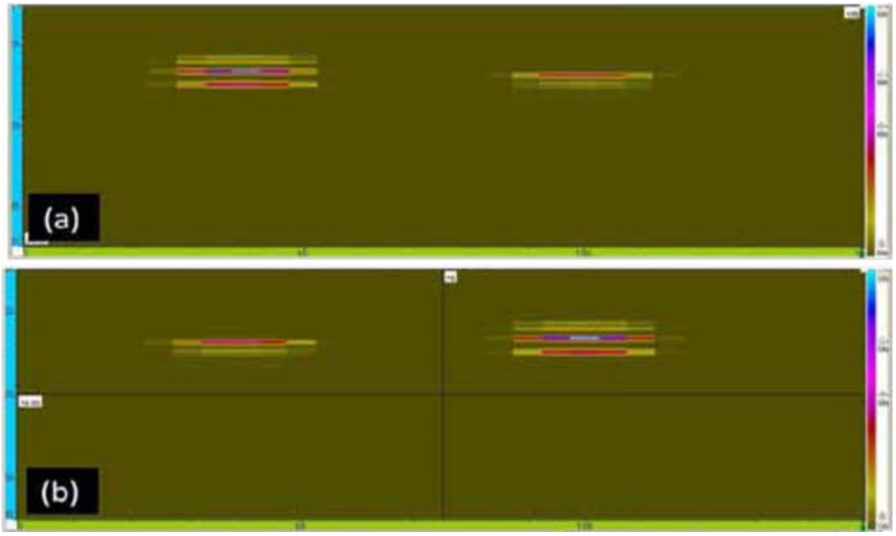

Figure 6 : Simulated B Scan images of LA probe (LW) scanned from (a) P91 side and (b) Ally 800 side

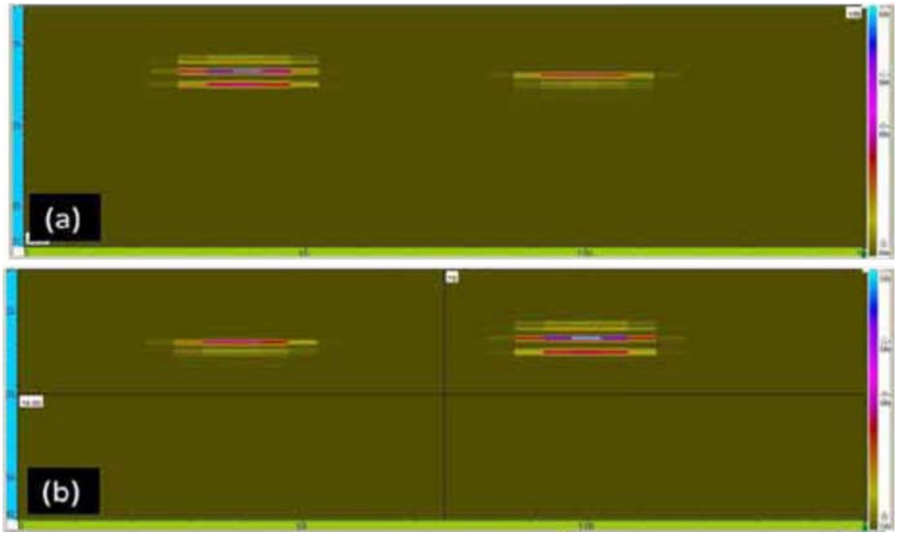

Figure 7 : Simulated B Scan images of DMA probe (LW) scanned from (a) P91 side and (b) Alloy 800 side

Microstructure

The microstructure of the base material Alloy 800 is shown in Figure 3 (a). The Alloy 800 has equiaxed grains of austenite with several twinning observed in the microstructure. It consists of microstructure with solid solution matrix in which some grains are outlined by the precipitate particles at the boundaries and by twining lines which are shown in Figure 3(a). The average grain size found by the mean intercept method is about coarser ASTM 5 (grain size-50 μm). The microstructure of the received base material P91 is shown in Figure 3(b). The microstructure of P91 consisted of tempered lath martensitic structures, as shown in Figure 3(b). The average grain size found by mean intercept method is about 24 μm as per ASTM No 8 method. The microstructures at the weld interfaces of the P91 side are shown in Figure 3(c). Coarse grain observed in the near weld zone of p91 side. Fine grain is observed away from the weld zone.

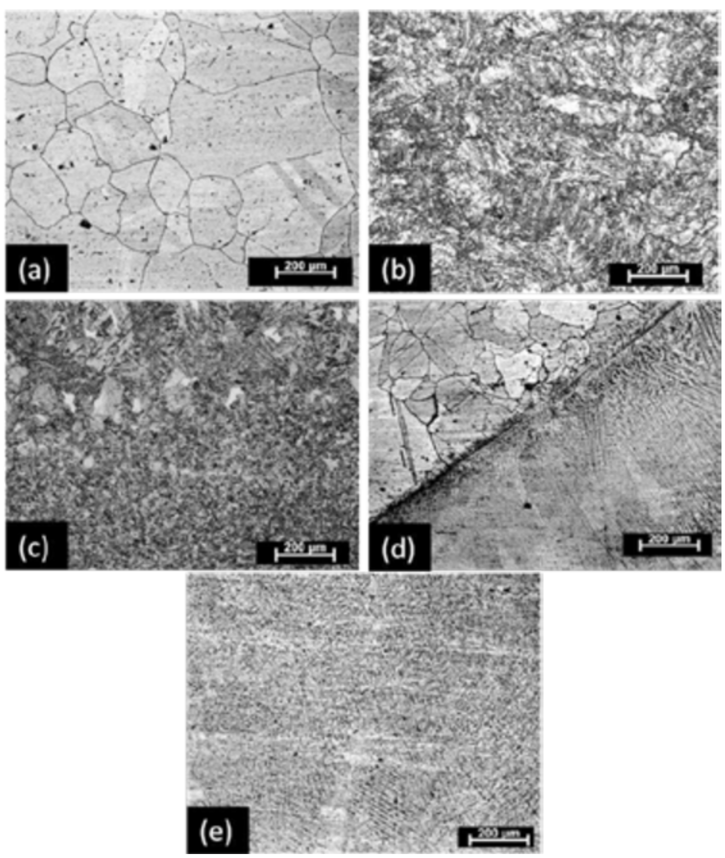

Figure 3 : Microstructure of the Alloy 800 (a) base metal (b) P91 base metal (c) Fusion boundary of P91 (d) Interface of Alloy800 to weld metal (e) Weld metal

The microstructures at the weld interfaces of Alloy 800 side are shown in Fig 3(d). Weld metal microstructures showed fine equiaxed grains on the Alloy 800 interface. Very large coarse grain is observed in the alloy 800 side in the range of 50 μm to 80 μm. The width of the HAZ is high compared to Alloy 800 side, because of the fact that the coefficient of thermal expansion (CTE) of austenite is being higher than that of ferritic, and the thermal conductivity of austenite being lower than the ferrite. Weld metal microstructure as shown in the figure 3(e). From the optical micrograph analysis it is clear that grain growth occurred from base metal to weld metal and the change in the microstructure of weld zone was analyzed. The dendritic structures were created by reheating and cooling during overlapped weld bead movement. The cooling rate ought to be the principle reason for the change in microstructure from cellular to dendritic because of low heat input which resulted from the higher cooling rate and therefore a finer microstructure. The microstructures in the fusion zone were formed due to solid phase transformation and solidification behaviour, which in turn were controlled by weld cooling rates and chemical compositions. This coarse crystallography-oriented grains and anisotropic structure affect the sound propagation in the weld metal to change the ultrasonic beam path, resulting in a worse signal-to-noise ratio. These factors cause an increase in the difficulty of the interpretation of the ultrasonic signal, which ends up being reflected in the loss of accuracy of the location and the dimensioning of the defects, thus making it difficult to distinguish between real defects and false indications [21].

Experimental Results

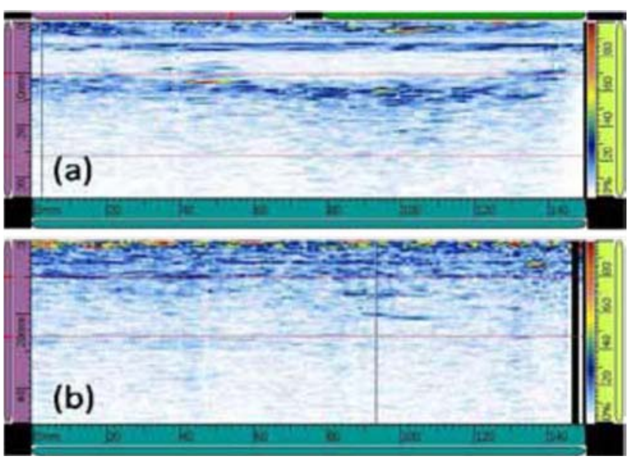

Figure 8 : Experimental B Scan images of LA probe (SW) scanned from (a) P91 side and (b) Alloy 800 side

Figure 8 shows the B scan image of inspections performed on a weld sample in P91 scanning side and alloy 800 sample using a linear array probe (with a solid wedge about 10 mm length) with shear wave. Defect 1 signal detected at 6.83mm depth with 40 db gain & Defect 2 is not detected while scanning from the P91 side. Defect 1 is not detected & Defect 2 signal detected at 5.98mm depth with 46 db gain scanning from the alloy 800 side. Alloy 800 has coarser grain microstructure compared to P91 material which has fine grain. So the higher gain is required for defect detection in Alloy 800 scanning side. Both the B scan images, the noise in the image is more due to the following phenomenon. Due to the smaller wavelength, the shear wave in the propagation mode is more affected by the material's microstructure. Due to the high elastic anisotropy, the ultrasonic attenuation is primarily due to the scattering. The sound that propagates between two media with different elastic properties has a limit on the amount of energy passing through the interface. The grain boundary scattering in elastically anisotropic material causes a quantifiable amount of energy to be dispersed at the boundary interface due to the high acoustic impedance mismatch between the base metal and weld metal [22,23,24].

Figure 9 shows three inspections performed on a weld sample in P91 scanning side and alloy 800 sample using a linear array probe (with a solid wedge about 10 mm length) with longitudinal wave. Defect 1 signal detected at 6.72mm depth with 44 db gain & Defect 2 is not detected while scanning from the P91 side. Defect 1 is not detected & Defect 2 signal detected at 5.8mm depth with 48db gain scanning from the alloy 800 side. Longitudinal wave is required higher gain for defect detection compared to shear wave due to wedge effect. The height of the wedge is higher compared to shear wave wedge. The main advantage of longitudinal wave is better penetration in the weld metal and less noise due to following phenomenon. The longitudinal wave mode is relatively less affected by the material's microstructure due to its large wavelength than the shear wave.

Attenuation is directly proportional to the material's grain size and indirectly proportional to the longitudinal wavelength, which results in less attenuation compared to the shear wave (the longitudinal wavelength is about twice the shear wavelength value). As longitudinal waves propagate into the weld metal, due to less acoustic impedance mismatch in the weld interface, the received amplitude of the spurious indications (noise) is less [25,26,27].

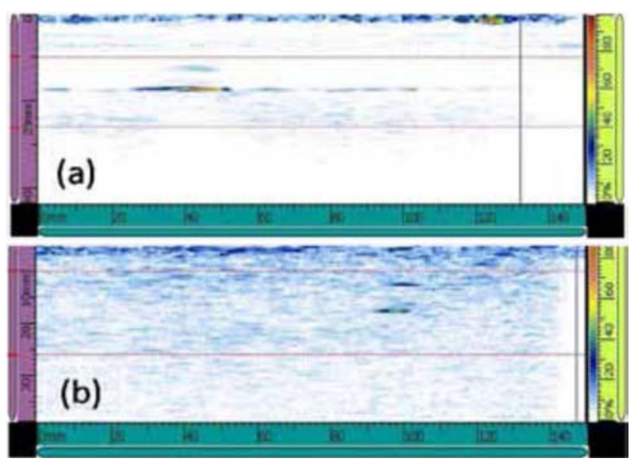

Figure 9 : Experimental B Scan images of LA probe (LW) scanned from (a) P91 side and (b) Alloy 800 side

Figure 10 shows three inspections performed on a weld sample in P91 scanning side and alloy 800 sample using a dual matrix array probe (with a solid wedge about 10 mm length) with shear wave. Defect 1 signal detected at 6.58mm depth with 35 db gain & Defect 2 is detected at 5.5mm depth with 38db gain for scanning from the P91 side. Defect 1 is

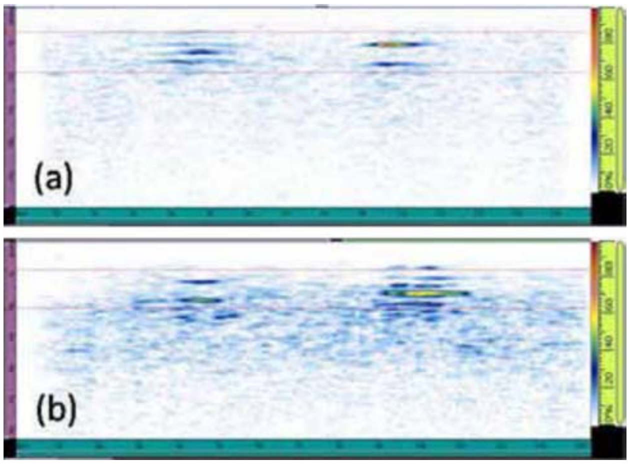

Figure 10 : Experimental B Scan images of DMA probe (LW) scanned from (a) P91 side and (b) Alloy 800 side

detected at 6.66mm depth with 36 db gain & Defect 2 signal detected at 5.65mm depth with 40db gain for scanning from the alloy 800 side. Less gain is required for detecting the both defects compared to LA probe due to the smaller wedge design generates less attenuation and enables the high focus depth in the material. The defects are clearly detected from the probes on the both side of the weld when scanning from the P91 side and Alloy 800 side. Due to the inclined design of the cross beam provides a pseudo focus, which increases the ability to detect more sensitive echoes. Use of a transmit-receiver (TR) probe reduces the near-surface dead zone as well as backscattering signals and eliminates "ghost echoes" caused by the wedge's internal reflections. Dual matrix array (DMA) longitudinal wave probes give low echoes of interference and penetrate better than shear waves. The pseudo focusing principle improves the signal to noise ratio and maintains the sound field better than single crystal transducers [28,29,30,31].

Defect Characterization

SNR Analysis

It is the ratio between the peaks of the signal to that of the noise. The peak amplitude of signal and noise is calculated from the A-scan image. The signal to noise ratio for DMA probe is higher than LA probe due to pseudo focusing of ultrasonic beam, less interference and wedge echoes. The signal to noise ratio noticed for shear wave examination is low compared to longitudinal wave due to energy scattered from the base and weld metal interface of dissimilar weld. From the table 4, it is observed that SNR is higher for DMA probe with longitudinal wave.

PROBES	LA Probe with SW		LA Probe with LW		DMA Probe with LW	
	EXP	SIM	EXP	SIM	EXP	SIM
P91	6.4	9.5	7.52	10.7	11	12.3
Alloy 800	5.9	7.8	7.34	9.9	9.6	11.2

Table 4 : Signal to noise ratio for different types of probes

Defect size and depth

Figure 11 shows the defect size calculation in the B scan image of ultrasonic testing for experiment and simulation. The size of the defect was determined by 6dB drop method obtained from the B-scan data. The analysis of the B-scan image and measuring the relative displacement of the probe position (at the maximum amplitude of the defect signals into half of the amplitude) as an indication of the size of the defect. Defect depth also found from the B scan images. The estimated defect sizes and defect depths are shown in the table 5 and table 6 respectively.

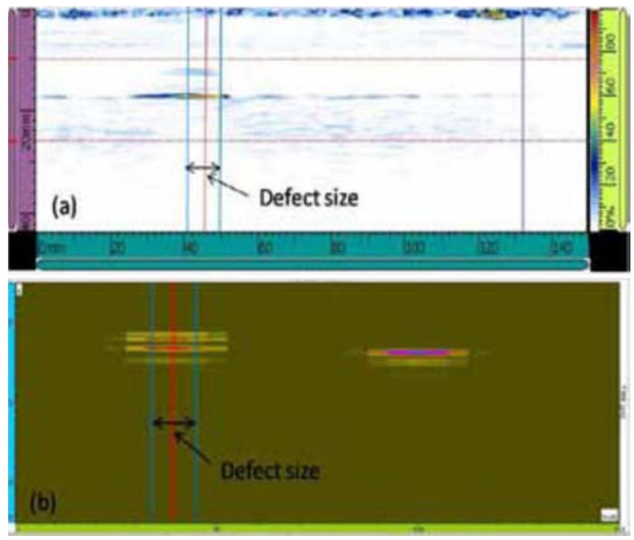

Figure 11 : Defect size calculation by 6dB drop method

PROBES	LA Probe with SW		LA Probe with LW		DMA Probe with LW	
Defects	P91	Alloy 800	P91	Alloy 800	P91	Alloy 800
Defect 1	8.55	ND	8.95	ND	8.8	8.9
Defect 2	ND	10.75	ND	11.50	11.30	11.35

ND – Not Detected

Table 5 : Defect size values for different types of probes

PROBES	LA Probe with SW		LA Probe with LW		DMA Probe with LW	
Defects	P91	Alloy 800	P91	Alloy 800	P91	Alloy 800
Defect 1	6.83	ND	6.72	ND	6.58	6.66
Defect 2	ND	5.98	ND	5.8	5.5	5.65

Table 6 : Defect depth values for different types of probes

Radiographic Evaluation

Defect size valuation was carried out for P91 to alloy 800 weld samples using ISEE software. Figure 12(a) shows the radiographic image of dissimilar weld and figure 12(b) line profile analysis of weld using ISEE software. Defect size calculation using radiographic image is shown in the table 7.

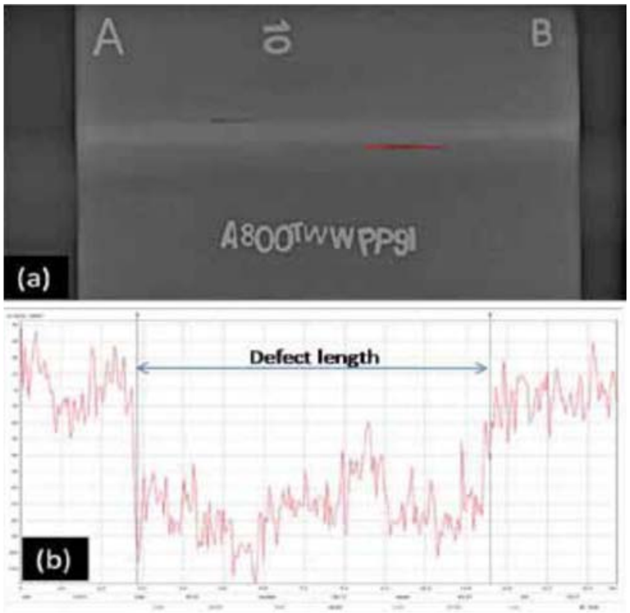

Figure 12 : (a) Radiographic images of dissimilar weld (b) line profile of defect region

Defects	Type of Defect	Size (mm)
Defect 1	Lack of sidewall fusion	8.67
Defect 2	Lack of sidewall fusion	11.1

Table 7 : Defect size values using radiographic images

PROBES	LA Probe with SW		LA Probe with LW		DMA Probe with LW	
Defects	P91	Alloy 800	P91	Alloy 800	P91	Alloy 800
Defect 1	1.4	ND	3.2	ND	1.5	2.65
Defect 2	ND	3.15	ND	3.6	1.8	2.25

Table 8 : Error percentage between the ultrasonic defect size and Radiographic defect size

The defect size comparison of LA probe with SW, LA probe with LW, DMA probe with LW is given in the table 8. From the table, it is observed that DMA probe gives less error percentage compared to LA probe for both defects. DMA probe improves the signal to noise ratio, Defect detection in dissimilar welds compared to LA Probes. Although, LA probe have some advantageous such easy to use, low cost, easy calibration etc.

Conclusions

This paper has presented simulations and experiments of the ultrasonic wave propagation and defect response performed on two different types of probes in dissimilar welds using model developed in CIVA software. Firstly, simulations of the ultrasonic propagation through dissimilar welds have been compared to the associated experiments with Signal to Noise Ratio. DMA probe show a better ability to detect defects than LA probe with a signal-to-noise ratio of 11, 12.3 for experiment and simulation respectively. The results of the simulation of the B-scan inspections show good agreement with the experimental results. The sizing of the defect in ultrasonic testing is calculated using 6dB drop method. The defect depth also found from the B scan images. The radiographic testing carried out for validating the defect location and defect sizing of experiment results. The error percentage between ultrasonic defect sizing and radiographic defect sizing is varied from 1.5 - 2.65 & 1.8 - 2.25 for Defect 1 and defect 2 respectively. The result of the simulation as well as experiments shows the dual matrix array probe gives the better defect detectability and beam propagation into the welds. This study confirms that the dual matrix probe is better suited for evaluating the dissimilar welds and also for coarse grain structure materials.

Acknowledgement

The authors are thankful to Dr. A. K. Bhaduri, Director, IGCAR for his encouragement and support. They also thank doctoral committee members for their guidance and motivation. The author also thanks Dr. Govind Kumar Sharma, Dr.K.Rajkumar, and Dr.R.Dhayalan for carrying out phased array ultrasonic simulation (CIVA software) and their valuable comments.

References

1. Bhaduri, A. K., & Laha, K. (2015). Development of Improved Materials for Structural Components of Sodium-Cooled Fast Reactors. Procedia Engineering, 130, 598-608
2. Mannan, S. L., Chetal, S. C., Raj, B., & Bhoje, S. B. (2003). Selection of materials for prototype fast breeder reactor. Transactions-Indian Institute of Metals, 56(2), 155-178.
3. Raj, B., Jayakumar, T., & Rao, B. P. C. (1995). Non-destructive testing and evaluation for structural integrity. Sadhana, 20(1), 5-38.
4. Szávai, S., Bézi, Z., Dudra, J., & Méhész, I. (2016). Modelling of phased array ultrasonic inspection of a steam generator dissimilar metal weld. Procedia Structural Integrity, 2, 1015-1022.
5. Lhémery, A., (2000) Modeling tools for ultrasonic inspection of welds. NDT & E International 33(7) 499-513
6. Ye, J., Kim, H. J., Song, S. J., Kang, S. S., Kim, K., & Song, M. H. (2011). Model- based simulation of focused beam fields produced by a phased array ultrasonic transducer in dissimilar metal welds. NDT & E International, 44(3), 290-296.
7. B Chassignole, O Dupond, L Doudet, V Duwig and N Etchegaray, (2009) 'Ultrasonic Examination of Austenitic Weld: Illustration of the Disturbances of the Ultrasonic Beam', 35th Review of Progress in Quantitative Nondestructive Evaluation, Vol. 28, pp 1886- 1893,
8. Gengembre, Nicolas, and Alain Lhémery. (2000) Pencil method in elastodynamics: application to ultrasonic field computation Ultrasonics 38(1-8) 495-499
9. Gengembre, Nicolas. (2003)Pencil method for ultrasonic beam computation Proc. of the 5th World Congress on Ultrasonics, Paris.

10. Lonné, S., (2006) Experimental validation of CIVA ultrasonic simulations International Conference on NDE in relation to structural Integrity for Nuclear and Pressurised Components.
11. Calmon, Pierre, (1997) "Integrated models of ultrasonic examination for NDT expertise." Review of Progress in Quantitative Nondestructive Evaluation, Springer, Boston, MA, 1861-1868
12. P. Calmon (2006) CIVA: an expertise platform for simulation and processing NDT data, Ultrasonics 44 975-979
13. N. Leymarie., (2013) Modeling of weld inspection by using a paraxial ray-tracing approach in a variable anisotropy medium, BINDT congress, July
14. K. Jezzine, (2013) Evaluation of ray-based methods for the simulation of UT welds inspection', 39th Review of Progress in QNDE', Vol 32B, pp 1073-1080
15. Mahaut, Steve, (2004) Simulation and application of dynamic inspection modes using ultrasonic phased arrays." AIP Conference Proceedings. Vol. 700. No. 1. AIP,
16. Toullelan, Gwénaël, (2008) Inspection of Complex Geometries using Flexible Phased-Array Transducers 17th World Conference on Nondestructive Testing, Shanghai, China.
17. Calmon, P., Mahaut, S., Chatillon, S., and Raillon, R. (2006) CIVA: An expertise platform for simulation and processing NDT data Ultrasonics 44975-979
18. Le Bourdais, F., Baqué, F., Baronian, V., and Reverdy, F. (2013) Design of ultrasonic inspection methods for sodium cooled reactors by CIVA simulation. In 2013 3rd International Conference on Advancements in Nuclear Instrumentation, Measurement Methods and their Applications (ANIMMA) 1-8
19. Roth, D. J., Tokars, R. P., Martin, R. E., Rauser, R. W., and Aldrin, J. C. (2009) Ultrasonic phased array simulations of welded components at NASA. In AIP Conference Proceedings 1096(1) 1190-1197
20. Gardahaut, A., Lourme, H., Jenson, F., Lin, S., & Nagai, M. (2014) Ultrasonic Wave Propagation in Dissimilar Metal Welds–Application of a Ray-Based Model and Comparison with Experimental Results. In Proceedings of the 11th European conference on non-destructive testing
21. Pudovikov, S., Bulavinov, A., & Kröning, M. (2008) Ultrasonic inspectability of austenitic stainless steel and dissimilar metal weld joints, 34. In MPA-Seminar Werkstoff-& Bauteilverhalten in der Energie-& Anlagentechnik (Vol. 9)
22. Kupperman, D. S., and Reimann, K. J. (1978) Effect of shear-wave polarization on defect detection in stainless steel weld metal Ultrasonics 16(1) 21-27
23. Kapranos, P. A., and Whittaker, V. N. (1983) Difficulties in the ultrasonic inspection of 316 austenitic steel welds arising from acoustic impedance mismatch Nondestructive Testing And Evaluation 1(3) 81-92
24. Lachance, F., Giguere, D., and Rioux, P. (2018) High Frequency Austenitic Stainless Steel Solution 12th ECNDT proceedings
25. Hudgell, R. J., and Seed, H. (1980) Ultrasonic longitudinal wave examination of austenitic welds British Journal of Non-Destructive Testing 22(2) 78-85
26. Hudgell, R. J., and Seed, H. (1980) The inspection of austenitic butt welds by longitudinal ultrasonic waves In Fourth international conference on pressure vessel technology 2
27. Kim, G. H., Park, C. K., Jin, S. W., Kim, H. S., Hong, K. H., Lee, Y. J., and Sa, J. W. (2016) Qualification of phased array ultrasonic examination on T-joint weld of austenitic stainless steel for ITER vacuum vessel Fusion Engineering and Design 109 1099-1103
28. Neumann, E., Kuhlow, B., Römer, M., and Matthies, K. (1976) Ultrasonic testing of austenitic components of sodium cooled fast reactors (No. IWGFR--10).
29. Edelmann, X., and Hornung, R. (1983) Investigation of an ultrasonic technique for detection of surface flaws during inservice inspection of dissimilar metal welds In Quantitative NDE in the nuclear industry
30. Ermolov, I. N., Razygraev, N. P., and Shcherbinskii, V. G. (1978) The use of head- type acoustic waves for ultrasonic monitoring. Soviet Journal of Nondestructive Testing 14(1) 27-33
31. Ohara, Y., Oshiumi, T., Nakajima, H., Yamanaka, K., Wu, X., Uchimoto, T., and Mihara, T. (2017) Ultrasonic phased array with surface acoustic wave for imaging cracks AIP Advances 7(6) 065214

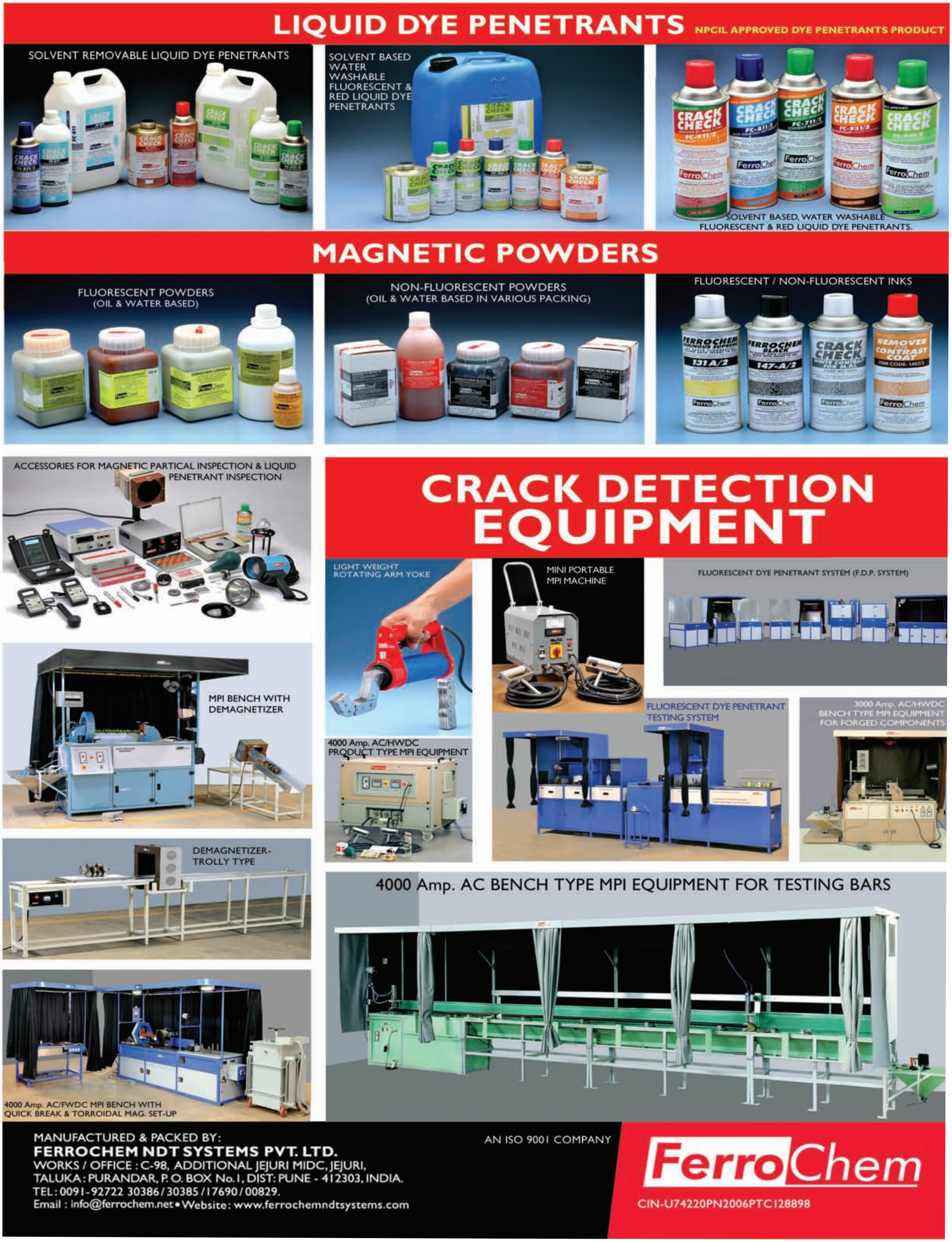

LIQUID DYE PENETRANTS
NPCIL APPROVED DYE PENETRANTS PRODUCT
SOLVENT REMOVABLE LIQUID DYE PENETRANTS
SOLVENT BASED WATER WASHABLE FLUORESCENT & RED LIQUID DYE PENETRANTS
SOLVENT BASED, WATER WASHABLE FLUORESCENT & RED LIQUID DYE PENETRANTS.
MAGNETIC POWDERS
FLUORESCENT POWDERS (OIL & WATER BASED)
NON-FLUORESCENT POWDERS (OIL & WATER BASED IN VARIOUS PACKING)
FLUORESCENT / NON-FLUORESCENT INKS
ACCESSORIES FOR MAGNETIC PARTICAL INSPECTION & LIQUID PENETRANT INSPECTION
CRACK DETECTION EQUIPMENT
LIGHT WEIGHT ROTATING ARM YOKE
MINI PORTABLE MPI MACHINE
FLUORESCENT DYE PENETRANT SYSTEM (F.D.P. SYSTEM)
MPI BENCH WITH DEMAGNETIZER
4000 Amp. AC/HWDC PRODUCT TYPE MPI EQUIPMENT
FLUORESCENT DYE PENETRANT TESTING SYSTEM
3000 Amp. AC/HWDC BENCH TYPE MPI EQUIPMENT FOR FORGED COMPONENTS
DEMAGNETIZER-TROLLY TYPE
4000 Amp. AC BENCH TYPE MPI EQUIPMENT FOR TESTING BARS
4000 Amp. AC/FWDC MPI BENCH WITH QUICK BREAK & TORROIDAL MAG. SET-UP
MANUFACTURED & PACKED BY:
FERROCHEM NDT SYSTEMS PVT. LTD.
WORKS / OFFICE : C-98, ADDITIONAL JEJURI MIDC, JEJURI,
TALUKA : PURANDAR, P. O. BOX No. I, DIST: PUNE - 412303, INDIA.
TEL : 0091-92722 30386 / 30385 / 17690 / 00829.
Email : info@ferrochem.net • Website : www.ferrochemndtsystems.com
AN ISO 9001 COMPANY
FerroChem
CIN-U74220PN2006PTC128898

NGC/NCB

NGC/NCB Office Bearer's List

NATIONAL GOVERNING COUNCIL MEMBER'S LIST (NGC)

1. Dr. B. Venkatraman
President – ISNT
Mob: 9443638974
bvenkat@igcar.gov.in
qadbvr@gmail.com

2. Shri Diwakar D. Joshi
President – Elect -ISNT
Mob: 9822263475
diwakarj@gmail.com

3. Dr. Krishnan Balasubramaniam
Vice President – ISNT
Mob: 9840200369
balas@iitm.ac.in

4. Dr. Jaiteerth R. Joshi
Vice President – ISNT
Mob: 9440049272
joshidrdl@gmail.com

5. Shri Rajul R. Parikh
Vice President – ISNT
Mob: 9820192953
rajulparikh@eecindia.com

6. Shri Samir K. Choksi
Hon. Gen. Secretary - ISNT
Mob: 9821011113
Choksiindia@yahoo.co.in
samir.choksi@choksiworld.com

7. Shri Bikash Ghose
Hon. Jt. Secretary - ISNT
Mob: 9890127524
bikashghose@gmail.com

8. Shri Nerurkar K.A
Hon. Treasurer - ISNT
Mob: 9822525518
pradeepndt@vsnl.net

9. Shri S. Viswanathan
Hon. Co-Treasurer –ISNT
Mob: 9894945482
viswa@igcar.gov.in

10. Shri R.J. Pardikar
Immediate Past President – ISNT
Mob: 9003096843
r.j.pardikar@gmail.com

MEMBERS

11. Shri Anil V. Jain
12. Shri Anandan. P
13. Shri V. Deepesh
14. Shri Dharmveer Singh
15. Shri R.G. Ganesan
16. Prof. S. Gopalakrishnan
17. Shri S. Hari Krishna
18. Shri G. Levin
19. Shri V. Manoharan
20. Shri P. Mohan
21. Shri Mukesh Arora
22. Ms. Menaka. M
23. Ms. Navita Gupta
24. Shri Bhausaheb Krishnaji Pangare
25. Shri Partha Pratim Brahma
26. Dr. Ravibabu Mulaveesala
27. Shri Sadasivan. N
28. Ms. Sangita Kapote
29. Shri Shashidar Pallaki
30. Shri M. S. Shendkar
31. Shri Uday Kale
32. Shri Umakanthan Anand
33. Dr. Venugopal. V
34. Shri M.N.V. Viswanath
35. Shri M.S. Viswanathan
36. Shri R. Vivek

PERMANENT INVITEE

37. Shri G. Ramachandran

PAST PRESIDENTS

38. Shri V.R. Deenadayalu
39. Shri K. Balaramamoorthy
40. Shri Ramesh B. Parikh
41. Shri A. Srinivasulu
42. Dr. Baldev Raj
43. Shri D.M. Mehta
44. Shri K. Viswanathan
45. Shri S. I. Sanklecha
46. Shri Dilip P. Takbhate
47. Shri K. Thambithurai
48. Dr. P. Kalyanasundaram
49. Shri V. Pari
50. Shri D.J. Varde

EX-OFFICIO MEMBERS

51. Dr.M.T.Shyamsunder-
Chairman,NCB
52. Dr. P. P. Nanekar
Hon.Secretary–NCB-ISNT
53. Shri S.Viswanathan
Hon.Treasurer–NCB-ISNT
54. Shri T. Loganathan
Controller of Examinations, NCB - ISNT
55. Dr. Krishnan Balasubramaniam
President - QUNEST Foundation
56. Shri V. Pari
Member-Secretary,QUNESTFdn.
57. Dr. P. Kalyanasundaram
Hon.Treasurer–QUNEST–Fdn.

NATIONAL CERTIFICATION BOARD MEMBER'S LIST (NCB)

1. Dr. M.T. Shyamsunder
2. Shri P.P. Nanekar
3. Shri T. Loganathan
4. Shri S. Viswanathan

REGIONAL CONTROLLER OF EXAMS

5. Shri A.K. Chandra
6. Shri S.R. Ravindran
7. Shri Jayaprakash Hiremath

PATRON

8. Shri K. Balaramamoorthy

MEMBERS

9 Shri. R.B. Bhardwaj
10. Shri V. Manoharan
11. Shri Avinash U. Sonawane
12. Shri R. Sundar
13. Shri Phani Babu
14. Shri Dilip Gatti
15. Shri ME. K.A Nerurkar
16. Shri Bikash Ghose
18. Shri Chintamani Khade
19. Shri G.V.S. Hemantha Rao
20. Shri. Uday B Kale
21. Shri Sadasivan. N
22. Shri. Vikas Neeraj
23. Smt. Navita Gupta
24. Shri M. Venkata Reddy

EX-OFFICIO MEMBERS

25. Dr. B. Venkatraman
26. Shri Diwakar D. Joshi
27. Dr. Krishnan Balasubramaniam
28. Shri. Jaiteeth Joshi
29. Shri. P. Mohan
30. Shri Nerurkar K.A
31. Shri. V. Pari

CHAPTER REPRESENTATION

32.Dr. Paritosh Nanekar
33. Mr. G. Ramachandran
34. Mr. Sunil Gophan
35. Dr. Jaiteerth Joshi